Merentutkimuslaitos
Havsforskninginstitutet
Finnish Institute of
Marine Research

WORKSHOP ON MODELLING OF THE MARINE-ATMOSPHERIC BOUNDARY LAYER

Helsinki 7-8 December 1998

PROCEEDINGS

Heidi Pettersson and Laura Rontu (eds.)




No. 40
1999

MERI
Report Series of the Finnish
Institute of Marine Research

MERI - Report Series of the Finnish Institute of Marine Research No. 40, 1999

Cover photos: Jan-Erik Bruun, Pekka Kosloff and Heidi Pettersson.

Publisher:
Finnish Institute of Marine Research
P.O. Box 33
FIN-00931 Helsinki, Finland
Tel: + 358 9 613941
Fax: + 358 9 61394 494
e-mail: surname@fimr.fi

Julkaisija
Merentutkimuslaitos
PL 33
00931 Helsinki
Puh: 09-613941
Telekopio: 09-61394 494
e-mail: sukunimi@fimr.fi

Copies of this Report Series may be obtained from the library of the Finnish Institute of Marine Research.

Tämän raporttisarjan numeroita voi tilata Merentutkimuslaitoksen kirjastosta.

ISSN 1238-5328 ISBN 951-53-2078-X

MERI - Report Series of the Finnish Institute of Marine Research No. 40, 1999

WORKSHOP ON MODELLING OF THE MARINE-ATMOSPHERIC BOUNDARY LAYER

Helsinki 7-8 December 1998

PROCEEDINGS

Heidi Pettersson and Laura Rontu (eds.)

FOREWORD

Improved safety and economy of navigation is the aim of a cooperative research project initiated by the Finnish Ministry of Transport and Communications. The project is being realized by the Finnish Meteorological Institute (FMI) and the Finnish Institute of Marine Research (FIMR). Improved parametrizations and coupling of the atmospheric, wave, ocean circulation and ice models should lead to more reliable forecasts at sea. As a part of the project, the FMI and the FIMR organized a workshop on the modelling of the marine-atmospheric boundary layer. The workshop brought together specialists working with interactions between air, sea and ice to discuss the parametrization of the marine-atmospheric boundary layer.

Over a period of one and a half days we heard 14 interesting presentations about the effect of grid sizes, different parametrization schemes and improvements of models as well as related problems. One of the main issues of the workshop was the modelling of the Baltic Sea. The shape and size of the Baltic Sea and the structure of the coastline in its northern parts are demanding features in a correct modelling of the atmospheric-marine system. In winters, at least, part of the Baltic Sea is covered by ice. The ice, which is sometimes moving quite rapidly, forms ridges and opens leads, giving its contribution to the fluxes between air, sea and ice. One of the key issues was the grid size of the models and how to handle the important aspects of air-sea-ice interactions at the problematic broken coast line. The widely used Charnock "constant" and its value excited a lot of discussion. Wind and wave-dependent parametrization schemes for drag are now receiving increased attention with a more physical approach. Relevant and careful field measurements for validitation become more and more important as we approach the fine tuning of the models.

Coupling models to interact with each other raises many questions, as some of the parameters have different importance in different models. Proper handling of the interacting parameters improves the performance of the coupled models. This in turn demands further work in both the theoretical and experimental fields for gaining a deeper understanding of the physical properties of the challenging and multiform interactions between air, sea and ice.

The papers of 12 presentations are published in this report. We wish to express our gratitude to the participants, to the Finnish Ministry of Transport and Communications, to the staff of the Finnish National Archives and to Päivi Mikkola, FMI.

Heidi Pettersson
Finnish Institute of Marine Research

Laura Rontu
Finnish Meteorological Institute

CONTENTS

WORKSHOP ON MODELLING OF THE MARINE-ATMOSPHERIC BOUNDARY LAYER

December, the 7th - 8th, 1998
Finnish National Archives, Helsinki

AGENDA

Monday 7.12.1998

Chairman Carl Fortelius

09.30-09.45 Opening of the workshop, Mikko Alestalo (FMI)

09.45-10.15 Sergei Kitaigorodskii (FMI): "Aerodynamic roughness of the sea surface as seen from above and from below - do we need them in modelling of the marine atmospheric boundary layer"

10.15-10.45 Coffee

10.45-11.10 Priit Tisler and Carl Fortelius (FMI): "Verification of HIRLAM marine boundary layer winds"

11.10-11.35 Laura Tuomi, Kimmo Kahma and Heidi Pettersson (FIMR): "WAM forced by mesoscale FMI HIRLAM in the Baltic Sea- preliminary results"

11.35-12.00 Ann-Sofi Smedman (MIUU): "Is the logarithmic wind law valid over the sea?"

12.00-13.30 Lunch

Chairman Kalle Eerola

13.30-13.55 Ulf Högström, Ann-Sofi Smedman, Hans Bergström and Anna Rutgersson (MIUU), Kimmo Kahma and Heidi Pettersson (FIMR): "The marine boundary layer during swell according to recent studies in the Baltic Sea."

13.55-14.20 Hannu Savijärvi (DMUH): "Marine ABL and the UH Mesoscale modelling projects."

14.20-14.45 Discussion

14.45-15.15 Coffee

Chairman Timo Vihma

15.15-15.40 Jouko Launiainen, Bin Cheng and Timo Vihma (FIMR): "Air-ice coupling and thermodynamic modelling of sea ice"

15.40-16.05 Timo Vihma, Juha Uotila and Jouko Launiainen FIMR):"Observations and modelling of the atmospheric boundary layer over sea ice"

16.05-16.30 Jari Haapala (DGUH): "Modelling of the Baltic Sea ice thickness distribution"

16.30-17.30 Discussion

19.00 - Dinner

Tuesday 8.12.1998

Chairman Kimmo Kahma

09.00-09.25 Tapani Stipa (DGUH): "On the (non)conservation of mass in PE models"

09.25-09.50 Anna Rutgersson (SMHI/MIUU): "Measured and modelled latent heat flux over the Baltic Sea."

09.50-10.20 Coffee

10.20-10.45 Vladimir Makin (KNMI): "Coupling waves with the atmosphere - consequence on heat flux".

10.45-11.10 Veniamin Perov (SMHI) and Vladimir Makin (KNMI): "On the wind speed dependence of sensible and latent heat exchange coefficients over sea in the 3-D HIRLAM"

11.10-11.35 Niels Woetman Nielsen (DMI): A revised formulation of surface fluxes over sea in HIRLAM

11.35-12.55 General discussion and conclusions of the workshop

12.55 Closing of the workshop

13.00-16.00 The seminar room is available for continued discussions

MIUU	Department of Earth Sciences, Uppsala University, Sweden
KNMI	Royal Netherlands Meteorological Institute
SMHI	Swedish Meteorological and Hydrological Institute
DMI	Danish Meteorological Institute
DMUH	Department of Meteorology, Helsinki University, Finland
DGUH	Department of Geophysics, Helsinki University, Finland
FIMR	Finnish Institute of Marine Research
FMI	Finnish Meteorological Institute

PREFACE

The Baltic Sea area is characterized by a complex combination of land, sea and archipelago with open sea areas of varying dimensions and dense island networks. This represents a very demanding environment for any model trying to describe and predict the atmospheric and oceanic conditions in the area. The small-scale features that the sea and the boundaries cause in the atmospheric flow require a very high model resolution. Accurate forecasting of marine winds, for example, forms a central problem. Similarly, oceanic models have to be able to resolve details of the flow as well as wind waves and the dynamics and thermodynamics of sea ice in the spatially varying environment and variable atmospheric forcing. At present, the models allow for a realistic treatment of the exchange between the sea and atmosphere, as available computer power has now made it possible to use sufficiently high resolution in the models. It has thus become important to also increase the exchange of knowledge and views between oceanographers and atmospheric researchers. The present workshop is a step in that direction.

Mikko Alestalo

Finnish Meteorological Institute

AERODYNAMIC ROUGHNESSES OF THE SEA SURFACE AS SEEN FROM ABOVE AND FROM BELOW – DO WE NEED THEM IN MODELLING THE MARINE ATMOSPHERIC BOUNDARY LAYER?

S. A. Kitaigorodskii

Finnish Meteorological Institute, P.O. Box 503, FIN-00101 Helsinki, Finland

I ROUGHNESS FROM ABOVE (Z_0)

I 1.

Theoretical calculations of the drag of the sea surface are sometimes based on the balance between the turbulent and wave-induced stress. In this case, in order to determine the contribution of the turbulent part to the drag of the sea surface, the background (or local) roughness parameter must be prescribed (because the observable roughness parameter defines the total drag). The local roughness is usually assumed either to be as for an aerodynamically smooth surface (Makin & al., 1995) or according to the Charnock's expression with a proportionality constant chosen rather arbitrarily (Janssen, 1989). The choice of the Charnock's expression for background roughness requires a careful determination of the proportionality constant, which can be derived only by some filtering procedure of the field observations.

In most hydrometeorological situations the process of wave breaking prevents one from having a smooth type of background roughness, since it leads to the formation of sharp crests and flow separation, including the cases of spilling and plunging breakers. Makin & al. (1995) have attempted to include the contribution of flow separation effects into the wave-induced parts of the stress, even though it is not well justified.

I 2.

The crucial point in the calculation of the drag of the sea surface is what parametrized form of the wind wave spectrum has been chosen. Results of numerical calculations demonstrate their sensitivity to the form of the high-frequency, high-wave-number tail of the wave spectrum. Most of the authors (Chalikov & Makin, 1991, Makin & al., 1995) used the Phillips constant α as being wave-age dependent, i.e. $\alpha = (U_a/c_p)^n$, where the power exponent n takes the values 2/5, 2/3, 3/2 varying from weak to strong dependence of α on wave age (U_a–wind speed, c_p–phase velocity of wave spectral peak). However, in his recent works (Kitaigorodskii, 1992, 1998a), the author has been trying to prove that experimental data support more favourably the movement of the low-frequency boundary of the Phillips saturation subrange ω_g towards lower frequencies with fetch growth (Kitaigorodskii, 1998b) rather than the variability of the Phillips constant with wave age.

I 3.

In order to derive the background roughness in the above-mentioned models of surface drag, it seems reasonable to take the value of the Charnock constant from data corresponding to the initial stages of wave development, when microscale breaking is the dominant process in wave dissipation. To define the values of U_a/c_p, which can be used to pick up the background roughness, it is also possible to look at the U_a/c_p-values for which the dissipation in water approaches its wall-law values (Kitaigorodskii, 1997a).

I 4.

In theoretical calculations of heat and moisture fluxes (Makin & Mastenbroek, 1996 in the marine atmosphere boundary layer (MABL)), knowledge of the expressions for background (local) aerodynamic roughness is also needed for prediction of the Stanton number dependence on wind speed (Reynolds roughness number). But besides that, these calculations also require that the dependence of the local temperature roughness parameter on Reynolds roughness number Re_s and Prandtl number Pr must also be specified. This has been done using the analogy with heat transfer above solid aerodynamically smooth and rough surfaces (Kader & Jaglom, 1972, Kitaigorodskii, 1973). The modelling of the turbulent kinetic energy (TKE) balance in a wave-influenced MABL (Makin & Mastenbroek, 1996) with a given local thermal roughness shows the independence of the Stanton number on wind speed. This seems to agree with the most recent observations (HEXOS). Numerical calculations performed by the above authors also indicate that the contribution of the wave-induced part to the total heat flux is negligible. However, it must not be forgotten that these results, in the same way as calculations of the drag, are not only very sensitive to the parametrization of local aerodynamic and thermal roughnesses, but also critically dependent on the chosen empirical form of the wind input to waves (wave growth parameter) and the 2-D wind wave spectra.

I 5.

MABL modelling indeed requires knowledge about the variability of the total (observable) roughness parameter z_0, which according to all latest data (Kitaigorodskii & al., 1995, Makin & al., 1995), can be described with the Charnock constant being wave-age dependent. Such a dependence of the Charnock "constant" is very important in modelling the MABL since it indicates, through fetch dependence, the strong variation of roughness with wind direction. The HIRLAM model used by Myrberg (1997) is just one example of the importance of the influence of roughness variability with wind direction in predictions of the surface wind.

I 6.

Since the roughness parameter z_0 can be derived either from direct measurements of the friction velocity u_*, or from profile wind measurements, the question arises of what is the range of heights over which these methods of experimental determination of roughness are valid. The usual estimate of a constant stress layer $z_a << u_*/\Omega$, (Ω Coriolis parameter, u_* - friction velocity) is $z_a \sim 50$m, which is comparable or close to λ_p – the peak wave length. Thus, the region of constant fluxes can be influenced by wave-induced motions. However, both theory (Phillips, 1977) and numerical calculations (Chalikov & Makin, 1991) indicate that the "wave" boundary layer (WBL) height z_w is rather thin ($<< z_a$). This is partially a consequence of the well-known fact that the critical level z_c ($U_a(z_c) = c_p$) lies close to the surface for most stages of wave development. We can therefore expect the existence of a range of heights $z_w < z < z_a$ for which the usual definitions of u_* and z_o are applicable.

II ROUGHNESS FROM BELOW (Z_{OD})

II 1.

Attention was initially drawn to the parametrization of this parameter by Kitaigorodskii & Mälkki (1979) in connection with gas transfer (oxygen) in the MABL, and by Zilitinkevich (1991) in the parametrization of roughness for wind-drift surface currents. But only after Kitaigorodskii's works (1997b, 1994) did the physical meaning of this parameter and the methods for the description of its variability became clarified.

II 2.

The first natural application of z_{od} was in the modelling of the ocean boundary layer (OBL), where z_{od} is needed to calculate the structure of turbulence in the OBL. Usually, z_{od} appears in turbulence closure schemes through an expression for the vertical turbulent length scale $l = (z+z_{od})$. In models where the evolution of the MABL and OBL are considered together, it seems to me that z_{od} is needed as much as z_0. Examples of OBL modelling demonstrating the importance of the choice for the z_{od} parametrization can be found in Nogh & Fernando (1990), and especially in recent very interesting calculations by Graig & Banner (1994) and Graig (1996). These authors were able to demonstrate that enhanced values of dissipation and turbulent energy in the surface ocean layer cannot be explained without high values of z_{od}, a fact predicted in Kitaigorodskii's theory (1994, 1998c). (See also his review paper in Boreal Environment Research (Kitaigorodskii, 1998b)).

II 3.

Modelling of the MABL includes the problem of how to estimate the transfer of greenhouse gases, such as CO_2, between the atmosphere and the ocean. In the gas transfer theory developed by Kitaigorodskii (1984), it was shown that the transfer velocity $U_{tr} \sim (\nu\varepsilon_o)^{1/4}$, where ν is the kinematic viscosity and ε_o the surface value of dissipation of turbulent energy below wind waves. In a recent publication of the author (Kitaigorodskii, 1997c) it was shown that ε_o strongly varies with the wave age U_a/c_p due to the process of wind wave breaking (cf. lecture of Prof. Kitaigorodskii on 15 September 1998 at the Geophysical Society of Finland, devoted to the 100th anniversary of the birth of Prof. E. Palmén). With the observed range of values of ε_o, the expression $U_{tr} \sim (\nu\varepsilon_o)^{1/4}$ shows that U_{tr} can change by a factor of 2-3 (!) or even more, depending on the stage of wave development.

II 4.

Nevertheless, the wave age dependence of gas transfer is a very delicate question, even though the latest experimental data from nature (in particular oxygen and CO_2 fluxes) do show a strong dependence of gas transfer on wind waves' motion. Since $\varepsilon_o \approx u_*^4/K_o$ (K_o – shear free constant eddy viscosity) (Kitaigorodskii, 1998c) then $U_{tr} \approx u_*^{3/4} \nu^{1/4} / (z_{od})^{1/4}$ (u_* - friction velocity in water). This formula shows a rather weak dependence of U_{tr} on the wind speed U_a (u_* is roughly proportional to wind speed U_a). But because z_{od} can change by a factor of $10\text{-}10^3$ (Kitaigorodskii, 1994, 1998c), the theoretical prediction of the wind speed dependence of U_{tr} still remains an unsolved problem.

II 5.

Recent measurements of the kinetic energy dissipation rate ε below the sea surface emerged from the efforts of two well-planned specialised experimental programmes: WAVES (Water Air Vertical Exchange Studies) and SWADE (Surface Wave Dynamics Experiment) which have been analysed in Terray & al. (1996) and Drennan & al. (1996). Their methods of analysis of upper ocean turbulence data in the presence of breaking wind waves were revisited recently by Kitaigorodskii (1998c), allowing a determination of the variability of ε_o with wind wave generation conditions, and thus a solution of the problem of the determination of gas transfer velocities.

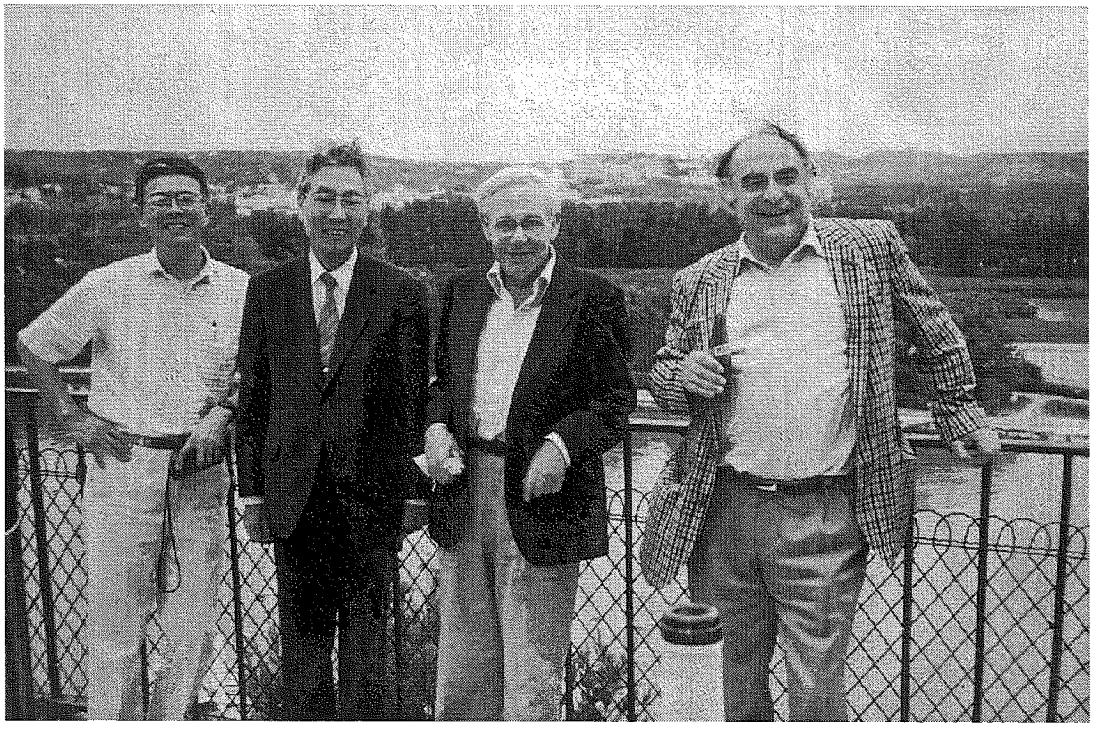

From the right: Prof. S.A. Kitaigorodskii, Prof. H. Charnock, Prof. Y. Toba and Dr. N.E. Huang. Workshop of SCOR Working Group 101, Avignon, France 1994.

REFERENCES

Chalikov, D.V & Makin, V.K. 1991: Models of the wave boundary layer. - Boundary-Layer Meteorology 53:83-99.

Drennan, W.M., Donelan, M.A, Terray, E.A. & Katasaros, K.B. 1996: Oceanic turbulence measurements in SWADE. - J. Phys. Oceanog. 26:808-815

Graig, P.D. 1996: Velocity profiles and surface roughness under breaking waves. - J. Geophys. Res. 101:1265-1277.

Graig, P.D. & Banner, M.L. 1994: Modeling wave enhanced turbulence in the ocean surface layer. - J. Phys. Oceanogr. 24:2546-2559.

Janssen, P.A.E.M. 1989: Wave-induced stress and the drag of air flow over sea waves. - J. Phys. Oceanogr. 19:745-754.

Kader, B.A. & Yaglom, A.M. 1972: Heat and mass transfer laws for fully turbulent wall flows. - Int. J. Heat Mass Transfer 15.

Kitaigorodskii, S.A. 1973: Air-sea interactions. - Israel program for scientific translations, Jerusalem, 237 pp. (Available as TT-72-50062 from U.S. National Technical Information Service, Springfield, V.A., 22151, USA).

Kitaigorodskii, S.A. 1984: On the fluid dynamical theory of turbulent gas transfer across an air-sea interface in the presence of breaking wind waves. - J. Phys. Oceanog. 14:960-972.

Kitaigorodskii, S.A. 1992: The dissipation subrange of wind wave spectra. Matematisk-fysiske Meddelelser. - Det Kongelige Danske Videnskabernes Selskab. The Royal Danish Academy of Sciences and letters, Munksgaard, Copenhagen, 42(5): 3-24.

Kitaigorodskii, S.A. 1994. A note on the influence of breaking wind waves on the aerodynamic roughness of the sea surface as seen from below. - Tellus 46A: 681-685.

Kitaigorodskii, S.A. 1997a: Dissipation subrange in nonlinear wind wave field and its role in the enhancement of the dissipation below breaking wave. - Dokl. Russian Acad. Sciences, 357(5): 690-692.

Kitaigorodskii, S.A, 1997b: The influence of wind wave breaking on the local atmosphere-ocean interaction. - Izv. Russian Academy of Science, Physics of Ocean and Atmosphere 33, p. 1-9.

Kitaigorodskii, S.A. 1997c: The influence of breaking wind waves on the aerodynamic roughness of the sea surface as seen from below. - Proceedings of Symposium on the air-sea interface and acoustic sensing, turbulence and wave dynamics. Marseille, (F), June 24-30, 1993, pp. 177-186.

Kitaigorodskii, S.A. 1998a: The dissipation subrange in wind wave spectra. - Geophysica 34(3): 179-207.

Kitaigorodskii, S.A. 1998b: Wind wave breaking and aerodynamic roughness of the air-sea interface as seen from above and below. - Boreal Environment Research 3:127-136.

Kitaigorodskii, S.A. 1998c: Towards the application of similarity theory to the description of the upper ocean turbulence. - Izv. Russian Academy of Science, Physics of Ocean and Atmosphere 34(3): 430-434.

Kitaigorodskii, S.A. & Mälkki P. 1979: Note on the parametrizations of turbulent gas transfer across an air-water interface. - Finnish Marine Research 246:111-124.

Kitaigorodskii, S.A., Volkov Yu. A. & Grachev, A.A. 1995: A note on the analogy between momentum transfer across a rough solid surface and the air-sea interface. - Boundary-Layer Meteorology 76:181-197.

Makin, V.K., Kudryavtsev, V.N. & Mastenbroek, C. 1995: Drag of the sea surface. - Boundary Layer Meteorology 73: 159-182.

Makin V.K. & Mastenbroek, C. 1996: Impact of waves on air-sea exchange of sensible heat and momentum. - Boundary-Layer Meteorol. 79:279-300.

Myrberg, K. 1997: Sensitivity tests of two-layer hydrodynamic model in the Gulf of Finland with different atmospheric forcing. - Geophysica 33(2): 69-98.

Nogh, Y. & Fernando, H.J.S. 1991: A numerical study on the formation of a thermocline in shear-free turbulence. - Phys. Fluids A.3(3): 422-427.

Phillips, O.M. 1977: Dynamics of the upper ocean, 2nd ed. - Cambridge University Press, 336 pp.

Terray, E.A., Donelan, M.A., Agrawal, Y.C., Drennan, W.M., Kahma, K.K., Williams III, A.J., Hwang, P.A. & Kitaigorodskii, S.A. 1996: Estimates of kinetic energy dissipation under breaking waves. - J. Phys. Oceanog. 26:792-807.

Zilitinkevich, S.S. (ed.), 1991: Modelling air-lake interaction. Physical Background. - Springer Verlag, Berlin, 129 pp.

VERIFICATION OF *HIRLAM* MARINE BOUNDARY LAYER WINDS

Priit Tisler & Carl Fortelius

Finnish Meteorological Institute, PO Box 503, FIN-00101 Helsinki, Finland

ABSTRACT

The present investigation aims at describing the systematic errors in near-surface winds predicted operationally at the Finnish Meteorological Institute (FMI). Comparisons of the predicted wind speed, using two different model versions, illustrate the effect of a larger continental influence on the coarser grid. A tendency to systematically overpredict the wind direction is observed.

1. *HIRLAM* AND DIAGNOSTIC CALCULATIONS OVER THE SEA

The operational short-range numerical weather forecast model at the FMI is based on the HIRLAM (HIgh Resolution Limited Area Model) version 2.5 (Källén, 1996). At the FMI, two versions of the HIRLAM model with different horizontal area and resolution are in operational use. Firstly, the main HIRLAM (ATL), with a gridscale of 0.4 degrees, covers Europe and the Northern Atlantic. Another version (EUR) produces forecasts for Northern Europe only with a horizontal resolution of 0.2 degrees, which translates to approximately 22 km. Both of them have 31 vertical levels and an identical number of grid points i.e. 194 x 140.

Boundary layer parametrization is based on the Monin-Obukhov theory of similarity. Surface fluxes of heat, momentum and water vapour are computed using drag coefficients that are functions of stability and a roughness length (Louis, 1979). Over the open sea the roughness length depends on wind speed (Charnock, 1955), over land and ice the roughness is constant in time.

Profiles of wind speed as well as of temperature and humidity in the surface layer are computed diagnostically using data from the lowest model level and boundary layer parameters including the surface characteristics. In grid squares containing both land and sea, the characteristics of the dominating surface type are used. This fact is important for the interpretation of model data especially over narrow seas and big lakes.

2. WIND MEASUREMENTS AND SOME RESULTS OF VERIFICATION

When the wind is blowing from land to sea it takes a considerable distance before a truly marine wind profile is established. Validation of marine winds should therefore ideally be based on offshore measurements uninfluenced by land and islands. In practice, such influences are felt for some wind directions at nearly all observing stations near the Finnish coastline. In addition, local obstacles also tend to influence the measurements. In the present study we have used observations that represent as closely as possible the conditions over open sea.

Wind measurements at sea are taken from anemometers mounted on buoys, ships, rigs and towers at heights ranging from 4.5 m (a buoy in the Bothnian Sea) to more than 50 m at some lighthouses. Usually, forecasts are made for a height of 10 m above the surface, but we have not attempted to adjust the observations to this reference height. Instead we used the model profiles to extract the wind at the height of each anemometer.

Figure 1 shows scatter diagrams of observed and predicted wind speeds in October 1998 at Kalbådagrund in the Gulf of Finland. The winds of the high-resolution model (EUR) are nearly unbiased with respect to the observations, whereas the low-resolution model (ATL) systematically underestimates the wind speed. The difference is explained by a larger continental influence on the coarser grid. At Kemi in the Bay of Bothnia, where both grids represent equally maritime conditions, both models perform equally well (Fig. 2).

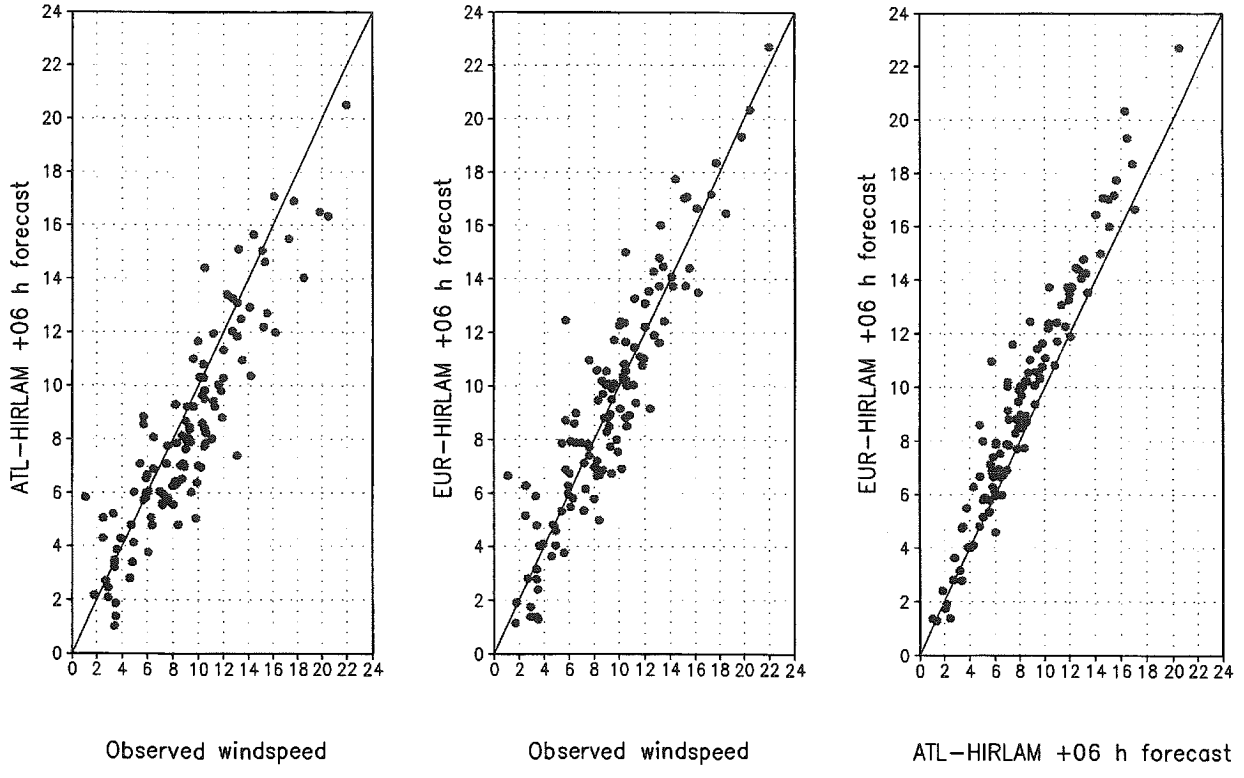

Fig. 1. Verification of HIRLAM winds (m/s) at Kalbådagrund, October 1998.

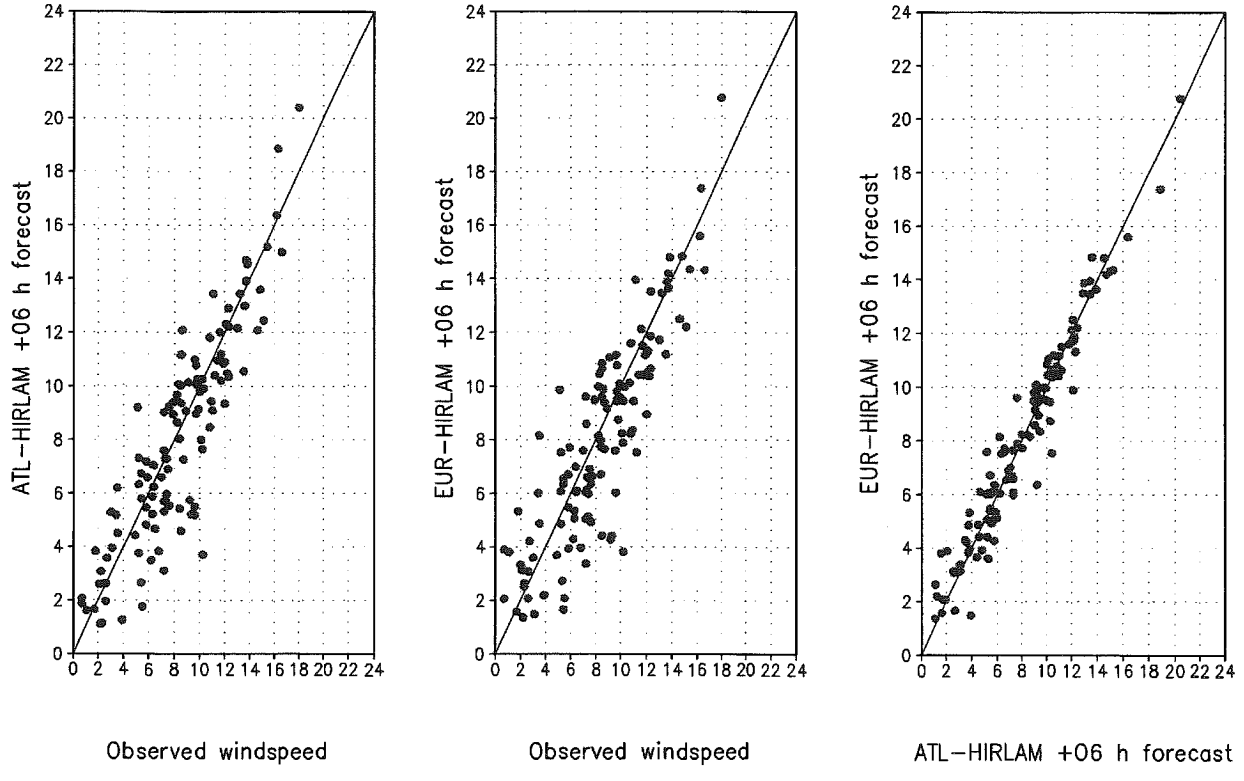

Fig. 2. Verification of HIRLAM winds (m/s) at Kemi, October 1998.

Figure 3 shows the observed and predicted (EUR) wind direction at four stations. A tendency towards overpredicting the wind direction is evident. The bias is caused by the tendency of the model to underestimate the frictional turning of the wind in the boundary layer. Although a slight shift in the wind direction is not crucial from the point of view of weather forecasting, the result nevertheless indicates a deficiency in the boundary layer parametrization. An incorrect turning of the wind may also affect the flow in the free atmosphere through Ekman pumping.

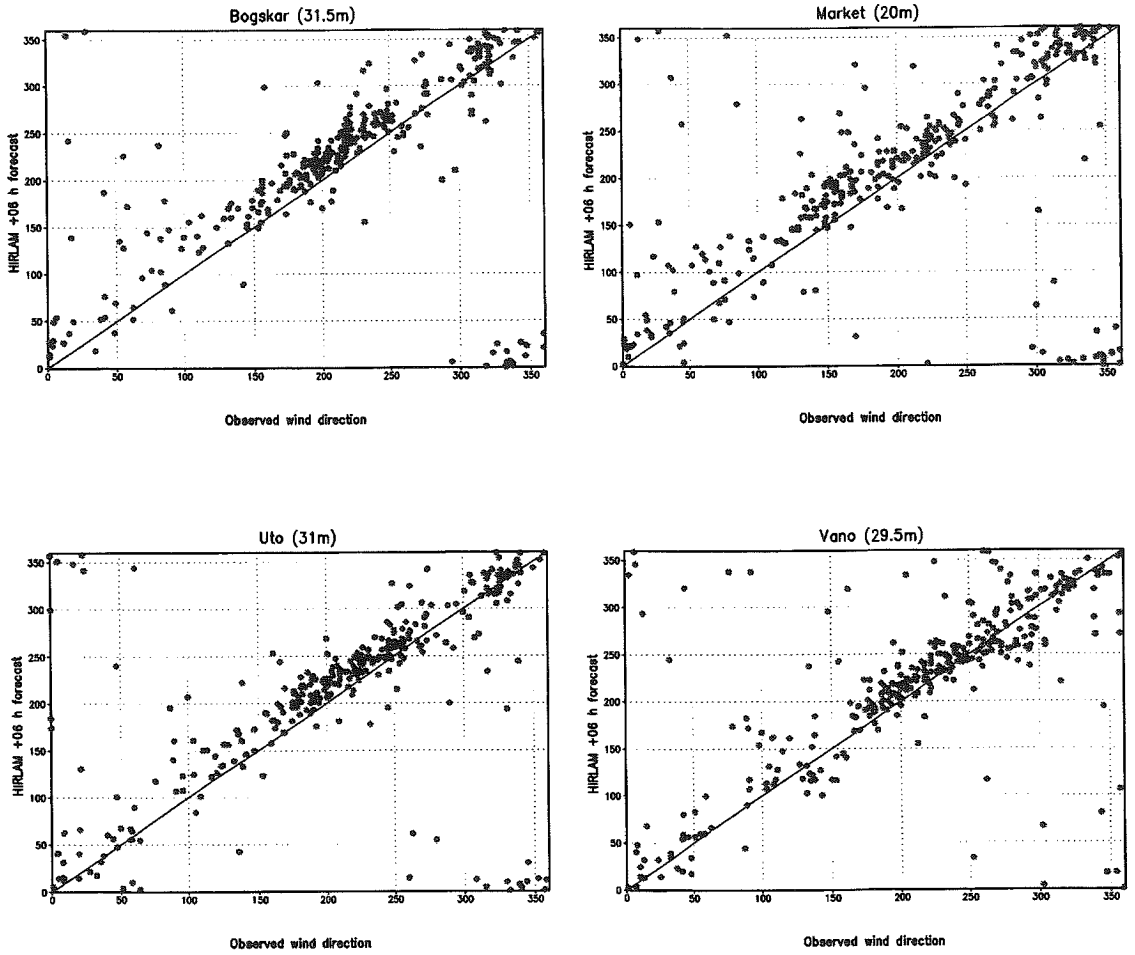

Fig. 3. Verification of HIRLAM (EUR) wind directions, June-July-August 1998.

REFERENCES

Källén, E. (ed.), 1996: HIRLAM documentation manual. - System 2.5. - Technical report, SMHI, Norrköping, Sweden.

Louis, J.F. 1979: A Parametric Model of Vertical Eddy Fluxes in the Atmosphere. - Boundary-Layer Meteorol. 17, 187-202.

Charnock, H. 1955: Wind stress on a water surface. - Quart. J. Roy. Meteor. Soc., 81, 639-640.

PRELIMINARY RESULTS FROM THE *WAM* WAVE MODEL FORCED BY THE MESOSCALE *EUR-HIRLAM* ATMOSPHERIC MODEL

Laura Tuomi, Heidi Pettersson & Kimmo K. Kahma

Finnish Institute of Marine Research
P.O. Box 33, FIN-00931 Helsinki, Finland

ABSTRACT

The WAM wave model forced by the Finnish Meteorological Institute's atmospheric EUR-HIRLAM model has been verified in the Baltic Sea. The resolution of EUR-HIRLAM (0.2 degrees) is less than half of the resolution of the HIRLAM model used in previous comparisons (0.5 degrees). The modelled significant wave heights were compared to the measurements made at two locations in the Baltic Sea. The reduction of the grid size of the atmospheric model improved the results significantly. The models perform well in the open sea, but results suggest that near the coast there still might be problems with the grid size and the numerical diffusion.

1. BACKGROUND

WAM is a third-generation wave model that has been developed by an international group of scientists over a ten-year period (Komen & al., 1994). WAM is based on the spectral energy balance equation, which equates the evolution of the wave spectrum to the sum of the local wind input, wave dissipation, nonlinear wave-wave interaction and the propagation of waves from nonlocal sources. HIRLAM (High Resolution Limited Area Model) is an atmospheric circulation model (Källén, 1996).

WAM was implemented for the Baltic Sea at the beginning of the 90's. Since then, several comparisons have been made with a one-way coupled WAM-HIRLAM combination as well as with a coupled version (Kahma & al., 1997). The results were unsatisfactory, especially when the waves were high.

The reasons for these failures in predicting the significant wave height correctly were identified as being the small size and shape of the Baltic Sea (Fig. 1) compared to the grid size of the atmospheric model. The archipelago in the northern part adds to the complications, because the conditions are simultaneously marine and terrestrial. The numerical diffusion in the atmospheric model that carries the effects of the higher surface roughness over land several grid points out to the sea, thus attenuating marine wind speeds, was also considered as one of the reasons (Cavaleri & al., 1997, Kahma & al., 1997).

The resolution of the atmosphere and that of the wave models were different in these comparisons. HIRLAM was on a rotated grid of 0.5 by 0.5 degrees (about 50 km) and WAM was on an unrotated grid of 0.1875 by 0.375 degrees (about 20 km). The winds supplied by HIRLAM had to be interpolated to the wave model's grid. Several methods, in addition to linear interpolation, were used: nearest points selected (no interpolation), 68 mid-sea points extrapolated to near-shore and land points, 39 mid-sea points extrapolated to near-shore and land points. These measures did improve the results, but not sufficiently.

In Fig. 2 are shown two examples of comparisons made with WAM forced by the Finnish Meteorological Institute's HIRLAM implementation. The results were compared to measurements made by a wave buoy at Kylmäpihlaja in 1992 and near Gotland in 1995 (Kahma & al., 1997) (Fig. 1). In both tests the modelled significant wave height followed the measured one quite well but completely missed the peaks of the high wind situations.

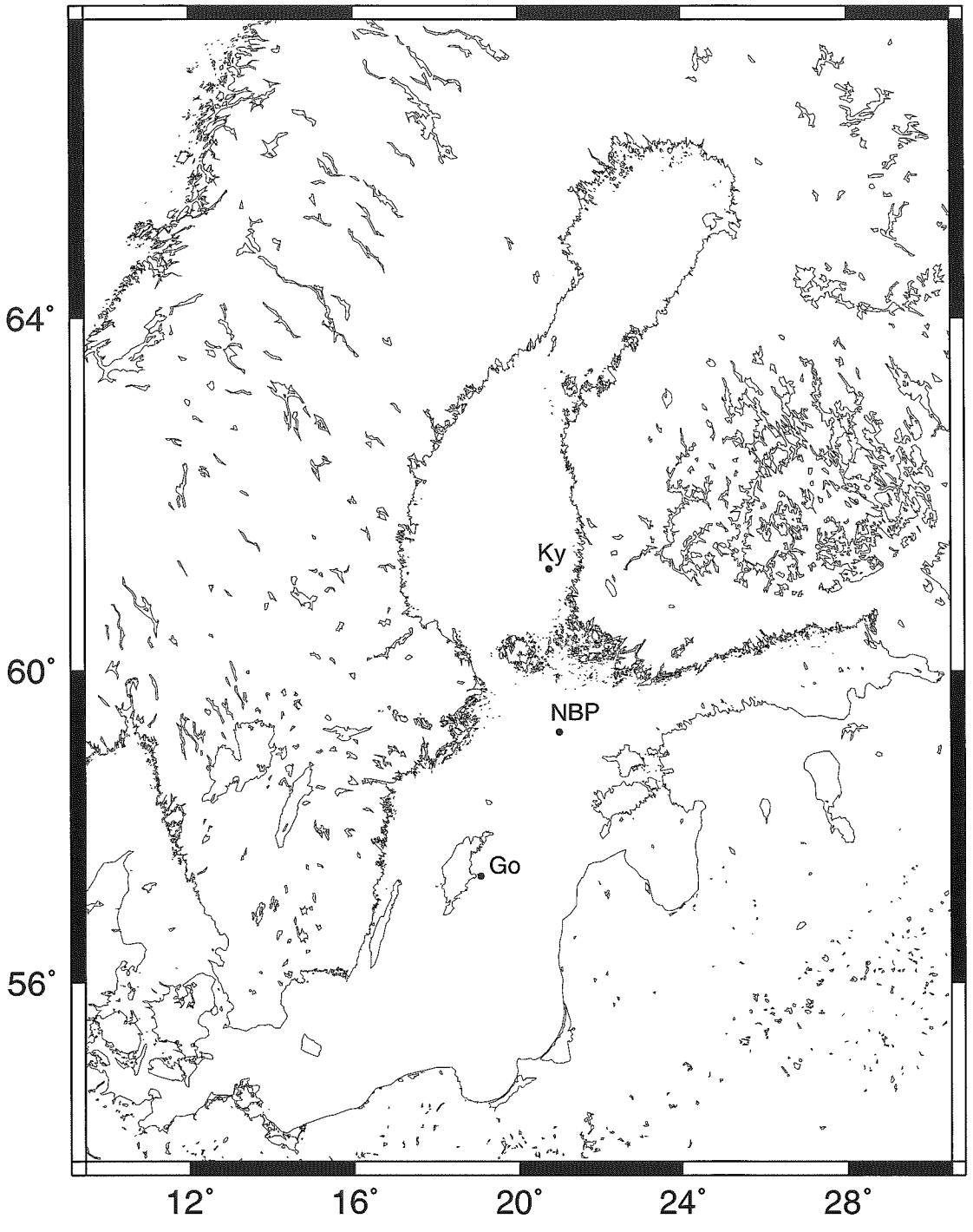

Fig. 1. Locations of the wave buoys in the Baltic Sea (Ky = Kylmäpihlaja, NPB = Northern Baltic Proper and Go = Gotland).

2. RESULTS WITH THE MESOSCALE *EUR-HIRLAM*

In 1998 comparisons were made with WAM forced by the 10 m surface wind supplied by the Finnish Meteorological Institute's new HIRLAM implementation at 6-hour intervals. The new EUR-HIRLAM is based on HIRLAM version 2.5 and it has the same resolution as the wave model, both being on a rotated grid of 0.2 by 0.2 degrees (about 20 km).

The modelled significant wave heights were compared to measurements made by two wave buoys, one to the east of the island of Gotland and the other in the middle of the northern Baltic Proper (Fig. 1).

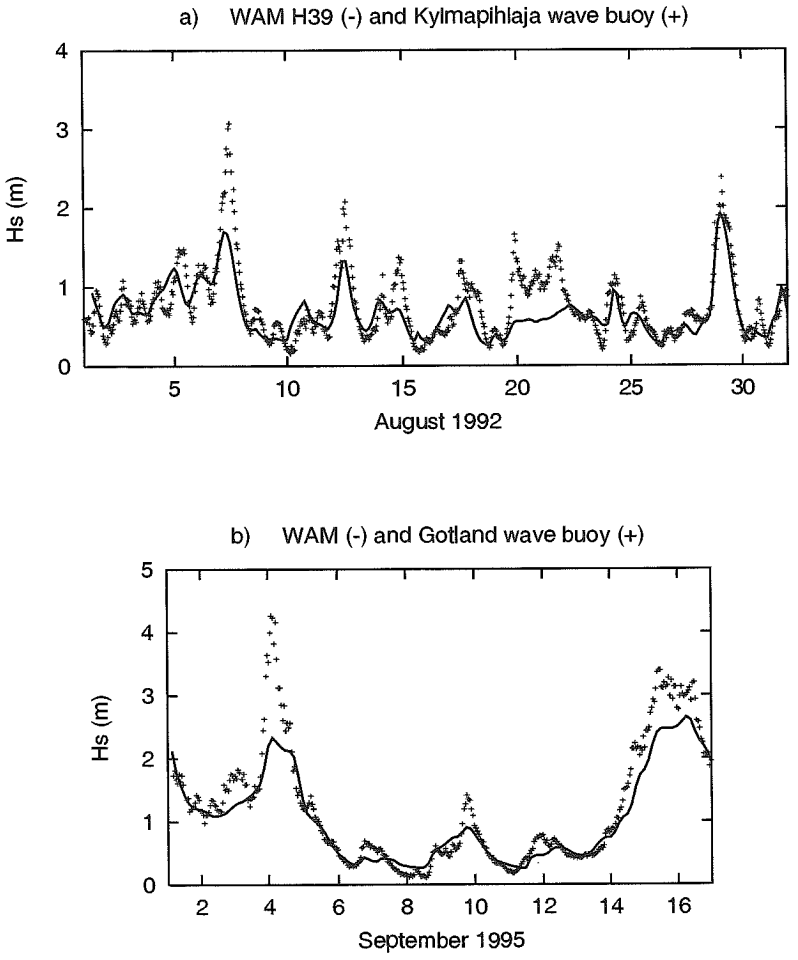

Fig. 2. Examples of the failures of the earlier versions: The modelled significant wave height compared to measurements made at Kylmäpihlaja (a) and near Gotland (b). The winds supplied by the Finnish Meteorological Institute's HIRLAM implementation are extrapolated to the wave model's grid using 39 mid-sea points (a) and 68 mid-sea points (b).

Using a smaller grid size in the atmospheric model should prevent the effects of the land being carried too far into the open sea, giving better results for the open sea, as long as the wind input and the physics of the wave model are correct. The comparisons in the northern Baltic Proper show a good agreement between the modelled and the measured significant wave height and also the peaks of the high wind situations in October are predicted quite correctly (Fig. 3). In general the significant wave height is still slightly underestimated by the model. There is only one noticeable failure, which is in the middle of August, when the wave model misses the peak by a factor of two. During the peak there is a large spatial gradient in the wind speed and direction in the northern Baltic Proper. It seems that the models have failed to predict this kind of situation correctly.

Near Gotland the results are satisfactory. The modelled wave height follows the measured wave height quite well but there are some problems with the peaks in the high wind situations (Fig. 4). The wave buoy is located near the coast of the island of Gotland but at a distance where the situation is marine. The nearest grid point the measurements can be compared to is about 10 km from the buoy towards the open sea. The over-predictions of the significant wave height occur as expected when the wind is blowing from the southwest (along the island), which was the case in October and in middle of July (Fig. 4).

In the comparisons made at the same location in 1995, the first high wind situation was from the southeast (from the open sea towards the island) and the significant wave height was underestimated by the model by a factor of two (Fig. 2, 4th September 1995) (Kahma & al., 1997).

With the reduced grid size, the results with southeast winds are much better, but the significant wave height is still a little underestimated by the model (Fig. 4, e.g. 14th and 28th August and 4th-5th and 8th October).

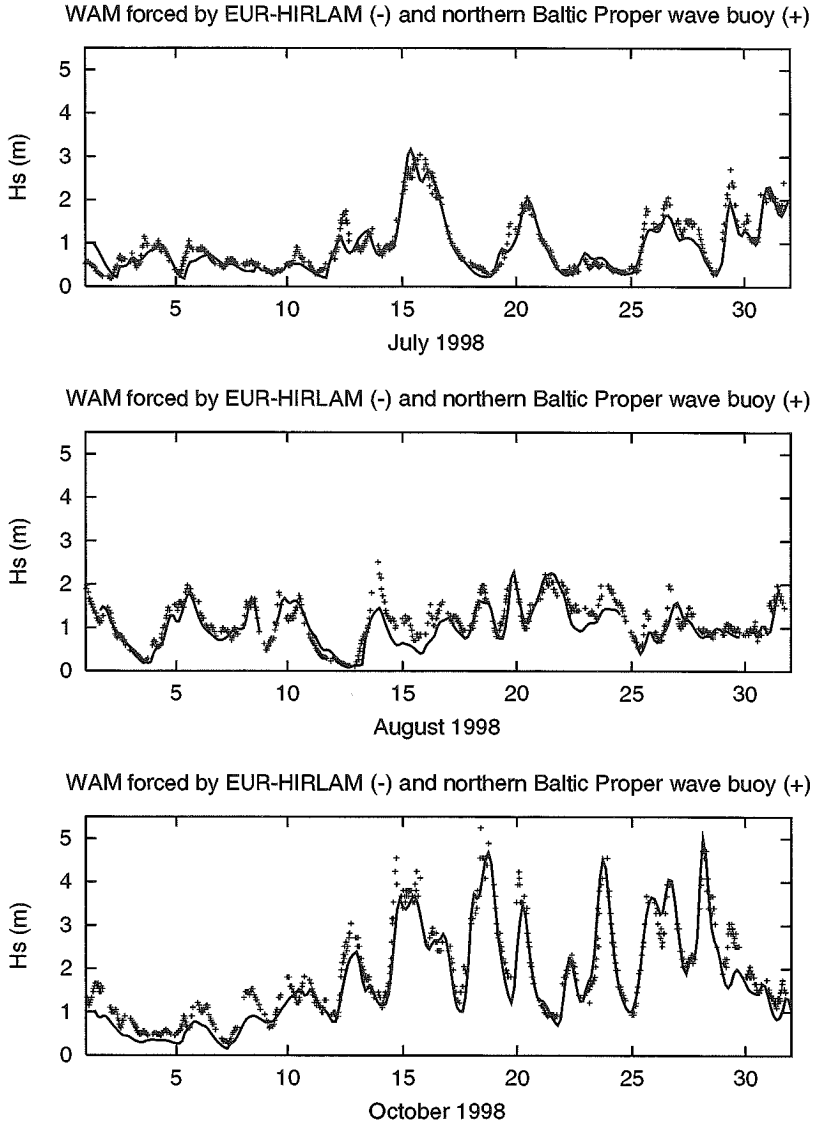

Fig. 3. The results from the WAM wave model forced by EUR-HIRLAM compared to the measurements made in the northern Baltic Proper. Note the greatly improved performance compared with Figure 2.

3. CONCLUSIONS

In this study comparisons between the modelled and measured significant wave heights in the Baltic Sea have been made. Reducing the grid size of the HIRLAM atmospheric model improved the performance of the WAM wave model significantly. The grid sizes of both models are now the same, so no interpolation of the wind is needed in the input. It seems that the best results can be obtained when the grid size of the atmosphere and wave model are the same.

The grid size of the atmospheric model of 0.2 degrees begins to be sufficient for open sea areas. The results from near the coast suggest that the grid size and numerical diffusion might still have an attenuating effect in these areas. This can cause problems in narrow bays like the Gulf of Finland. Besides this, the failure of the models to predict some turning wind situations demands further investigation.

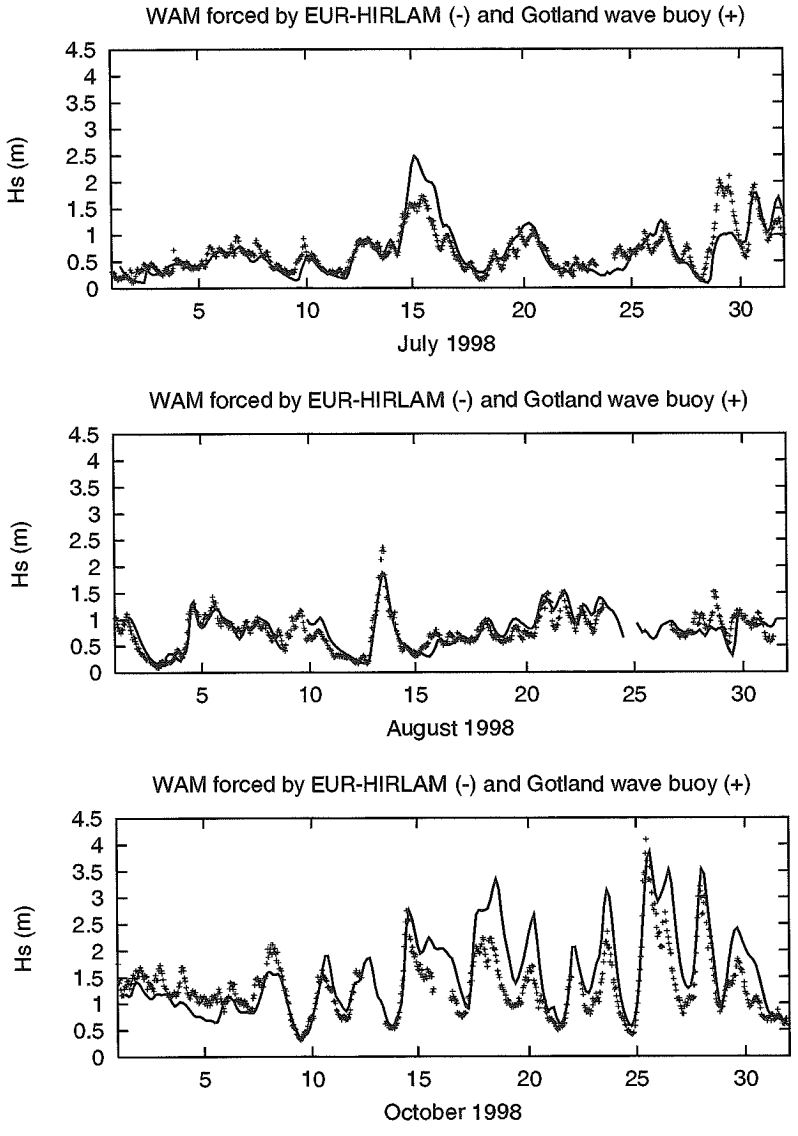

Fig. 4. The modelled significant wave height compared to the measurements made near Gotland.

Acknowledgements

This work has been supported by the Finnish Ministry of Transport and Communications.

REFERENCES

Cavaleri, L., Bertotti, L., Hortal, M., Miller, M. 1997: Effect of the reduced diffusion on surface wind and wave fields. - Monthly Weather Review 125, 3024-3029.

Kahma, K.K., Pettersson, H., Stipa, T., Högström, U., Smedman, A.S., Bergström, H. 1997: Comparison of wind stress hindcast by a coupled atmospheric-wave model (ECAWOM) and the measured wind stress at Östergarnsholm. Technical report. - Finnish Institute of Marine Research, Helsinki, 25s.

Komen, G.J., Cavaleri, L., Donelan, M., Hasselmann, K., Janssen, P.A.E.M. 1994: Dynamics and modelling of ocean waves. Cambridge Univ. Perss., 532s.

Källén, E. (ed.), 1996: Hirlam documentation manual: system 2.5. - Technical report, SMHI, Norrköping, Sweden. 240 s.

AIR-SEA INTERACTION DURING SWELL*

Ulf Högström, Ann-Sofi Smedman, Hans Bergström & Anna Rutgersson

Department of Earth Sciences, Meteorology,
Villavägen 16, S-752 36 Sweden

Kimmo K. Kahma & Heidi Pettersson

Finnish Institute of Marine Research
P.O. Box 33, FIN-00931 Helsinki

Air-sea interaction data from a situation with pronounced unidirectional swell have been analysed. Measurements of turbulence at three levels (10, 18 and 26 m above mean sea level) together with directional wave buoy data from the site Östergarnsholm in the Baltic Sea were used. The situation, which lasted for about 48 hours, appeared in the aftermath of a gale. The wind direction during the swell situation turned slowly within a 90 degree sector. Both during the gale phase and the swell phase the over water fetch was more than 150 km. The wind speed during the swell phase was typically 4 m s^{-1}.

The most striking features of the present study are the following: (i) When the wave age parameter c_o/U_{10} becomes larger than 1.2, the shearing stress at and near the surface becomes strongly suppressed, $-\overline{u'w'}$ having values smaller than 0.01 m^2 s^{-2}, the corresponding average C_D-value being about $0.7 \cdot 10^{-3}$. According to Pierson & Moskowitz (1964), $c_o/U_{10} = 1.2$ is the wave age at which the waves become fully developed. (ii) The turbulent intensities of all three velocity components remain high, so that the modulus of the correlation coefficient for u and w drops from its typical 'normal' value of about 0.35 to a value between 0.2 and 0, Figure 1. (iii) Most of the time there is a wind speed maximum below a height of 10 m above mean water level, a phenomenon interpreted as a wave-driven wind speed increase, Figure 2. (iv) The characteristic changes in the structure of turbulence mentioned under (ii) are observed equally clear at 10 and at 18 and 26 m. (v) The turbulence energy budget at 10 m is dominated by two gain-terms of approximately equal magnitude, pressure transport and buoyancy, whereas the local mechanical production and turbulent transport terms are numerically very small. (vi) Wave-related signatures in energy- and co-spectra are not very pronounced at any of the measuring levels. (vii) Quadrant analysis (see Smedman & al., 1999 for details) of the momentum flux shows that flux contributions from the interaction quadrants become almost as big as the sum of sweeps and ejections for high wave age conditions, making the net flux numerically small; no such corresponding effect is observed in quadrant analysis of the heat flux. Instead, the relative contribution of quadrant I to the transport process increases dramatically.

The above picture for the momentum flux is in general agreement with previous findings in similar situations (Volkov, 1970; Makova, 1975; Antonia & Chambers, 1980; Chambers & Antonia, 1981). Previous measurements were mainly confined to relatively low heights above the water surface, and in none of these studies were there simultaneous measurements of turbulent characteristics at several levels. Thus, it is a new finding of this study that the turbulence 'anomalies' during swell (compared to young wave conditions) are actually observed to occur in a layer extending to a height of at least 26 m. In fact, there are no indications in the data of a gradual decrease of the 'degree of anomaly' within this layer.

---

* The present text is an extended abstract of the following paper: Smedman, A., Högström, U., Bergström, H., Rutgersson, A., Kahma, K.K. & Pettersson, H. A case study of air-sea interaction during swell conditions. J. Geophys. Res., accepted, 1999.

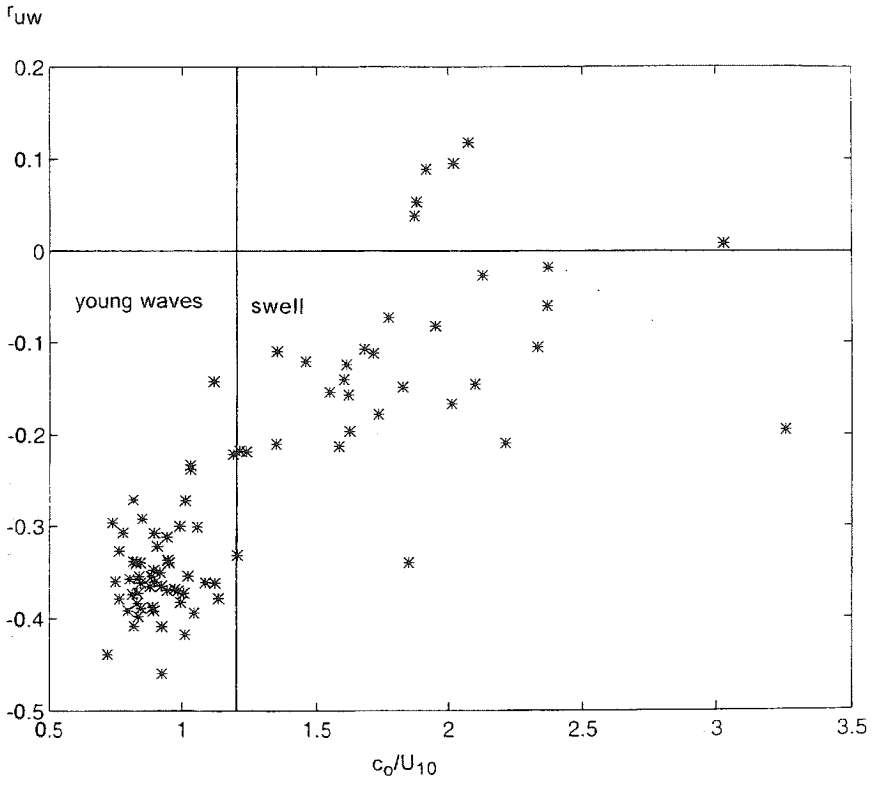

Fig. 1. Correlation coefficient $r_{uw} = \overline{u'w'}/(\sigma_u \cdot \sigma_w)$ for 26 m plotted as a function of the wave age parameter c_o/U_{10} (where 'c_o' has been calculated as weighted means over the flux footprint for the 26 m level, cf. Smedman & al., 1999).

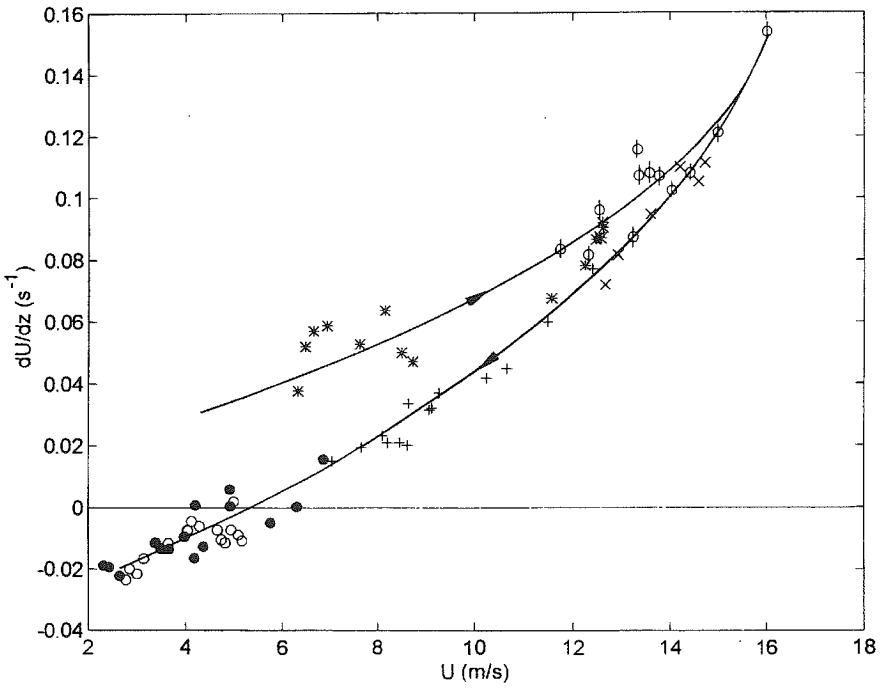

Fig. 2. Estimated values of hourly mean wind speed gradient at 10 m (determined from cup anemometer measurements at 5 levels) for the entire time period 14-19 September, 1995 plotted as a time sequence in the direction indicated by the arrows and as a function of wind speed at 10 m. Symbols: '*' 14 September; 'ϕ' 15 September; 'x' 16 September; '+' 17 September; '•' 18 September; 'o' 19 September. Note that negative gradients prevail during most of the swell period, 18-19 September.

It is reasonable to assume that in a shallow layer just above the undulating water surface there is, in the terminology of Belcher & Hunt (1993), an 'inner surface layer', which is governed by local momentum transfer from the air to the sea. In this layer it is also reasonable to assume that the ordinary wall-layer turbulence production mechanism is active (Kline & Robinson, 1989). At the same time, the longer waves (which travel faster than the wind) produce momentum transport by pressure fluctuations in the opposite direction. That such transport actually takes place, is clearly demonstrated by the quadrant analysis which shows that, for the momentum transport, the interaction quadrants become of increasing importance with increasing wave age, i.e. excess momentum is being transported upwards and deficit momentum downwards. At the same time, the heat flux is not at all affected in this way. Thus, momentum must be transported upwards from the surface by a mechanism which includes pressure - velocity correlations. Such a mechanism is not possible for transport of a scalar, such as virtual potential temperature which is studied here.

This situation creates a net momentum transport that is close to zero. This in turn means that there can be little local mechanical production of turbulence (because mechanical production = the product between the kinematic momentum flux and the local wind gradient). The net result of this state of affairs is that, in fact, there will be little 'active' turbulence in the boundary layer, except in a shallow 'inner surface layer' near the undulating water surface, leaving primarily the 'inactive' kind of turbulence, which is likely to originate primarily high up in the boundary layer. It is worth noting that during the present situation with swell, the number of individual 60-minute periods with negative net momentum flux (upwards directed flux) increases with height, being zero at 10 m, 3 at 18 m and 6 at 26 m. In the case studied in Smedman & al. (1994) the net momentum flux was found to be slightly negative in the lowest 200 m during a period of several hours.

The above sketch does not answer the question of how deep is the zone of direct wave influence and how deep is the 'inner surface layer'. The measurements of this study do not give very clear surface wave signatures in the spectra during the swell period - at the most there is a bulge and a plateau in the mean u- and w-spectra. At the same time, as shown in Figure 2, there is a wind maximum present somewhere below the lowest measuring point, 10 m, for most of the time during the swell period. From that it can be concluded that the 'inner surface layer' is certainly less than 10 m deep. A way of describing the situation would be to say that the bulk of the boundary layer is floating with very little friction on top of a layer limited in depth by this wind maximum close to the surface.

REFERENCES

Antonia, R.A. & Chambers, A.J. 1980: Wave-induced disturbances in the marine surface layer. - J. Phys. Oceanogr., 10:611-622.

Belcher, S.E. & Hunt, J.C.R. 1993: Turbulent shear flow over slowly moving waves. - J. Fluid Mech., 251:109-148.

Chambers, A.J. & Antonia, R.A. 1981: Wave-induced effect on the Reynolds shear stress and heat flux in the marine surface layer. - J. Phys. Oceanogr., 11:116-121.

Kline, S.J. & Robinson, S.K. 1989: Quasi-coherent structures in the turbulent boundary layer: Part I. Status report on a community-wide summary of the data. - Proc. Zoran Zaric Memorial Int. Seminar on near-wall turbulence. - Hemisphere, 200-217. Dubrovnik, Croatia.

Makova, V.I., 1975: Features of the dynamics of turbulence in the marine atmospheric surface layer at various stages in the development of waves. - Atmos. Ocean. Phys., 11:177-182.

Pierson, W.J. Jr. & Moskowitz, L. 1964: A proposed spectral form for fully developed wind seas based on the similarity theory of S.A. Kitaigorodskii. - J. Geophys. Res., 69:5181-5190.

Smedman, A.-S., Tjernström, M. & Högström, U., 1994: The near-neutral marine atmospheric boundary layer with no surface shearing stress: a case study. - J. Atm. Sci., 51:3399-3411.

Smedman, A., Högström, U., Bergström, H., Rutgersson, A., Kahma, K.K. & Pettersson, H., A case study of air-sea interaction during swell conditions. - J. Geophys. Res., accepted 1999.

Volkov, Yu. A., 1970: Turbulent flux of momentum and heat in the atmospheric surface layer over a disturbed sea-surface. - Izvestiya Acad. of Sciences, USSR, Atmos. and Oceanic Physics, 6:770-774.

THE MARINE ATMOSPHERIC BOUNDARY LAYER IN THE UNIVERSITY OF HELSINKI MESOSCALE MODEL

Hannu Savijärvi

Department of Meteorology
P.O. Box 4, FIN-00014 University of Helsinki, Finland

ABSTRACT

The University of Helsinki (UH) mesoscale model has been used for several sea-related studies. This short contribution gives a brief overview of the past and presently ongoing marine ABL-related research with this model, and specifically compares the HIRLAM turbulence scheme with the UH scheme over the sea. The UH model equations and its physical, computational and numerical details can be found from the given references.

1. INTRODUCTION; THE MODEL

The UH model is a two-dimensional sigma coordinate (i.e. hydrostatic) moist model with high vertical and horizontal resolution; 11-30 sigma levels in the boundary layer; Δx = 1-10 km. Horizontal advection is by Lagrangian cubic spline upstream interpolation and processes are time-split, updating their fields immediately. Large-scale conditions are given by the initial fields and by pressure gradients through the geostrophic wind, which is usually kept constant in time and space. Various boundary conditions can be used. The physics part includes a Monin-Obukhov-type surface layer, a vertical diffusion scheme based on the mixing-length approach as e.g. in HIRLAM, a fairly well-documented and accurate radiation scheme (4 bands in the solar, 6 bands in the thermal region), and horizontal diffusion via a weak low-pass filter. Cloud physics is also included. Surface temperatures are either specified, or predicted with a force-restore or a 5-level soil scheme. A version for planet Mars exists as well, being less relevant for marine ABL though. - At lake or sea surface points, temperatures are usually specified, and roughness lengths for momentum, heat and moisture are set at 0.1 mm. The lowest gridpoint height z_a is usually at about 2 m above the surface; however, the Mars "Pathfinder" version worked perfectly well with z_a as low as 0.33 cm (Savijärvi, 1999). The lowest layer is formally the surface layer in the model.

2. MARINE-RELATED MODEL STUDIES AND THEIR MAIN RESULTS

The first "marine" application of the UH model was the simulation of the typical vertical motions created near (Finnish) coasts through roughness changes and forced lifting by the coastal relief, when winds are blowing across or along the typical coastline in near-neutral conditions. The patterns of vertical motions helped to explain e.g. the observed snowdepth maxima near the coasts (Alestalo & Savijärvi, 1985). The sea breeze over a coastal city (Helsinki) was studied in Savijärvi (1985). A warm coastal city enhanced the sea breeze cell and locked it over the coastline. Sea breezes over steep coasts were discussed in Neumann & Savijärvi (1986). In model simulations the sea breeze jumped directly from over the sea to midslope, causing nearly calm conditions or even countercurrents above the coastline, as had been observed over really steep coasts e.g. in Chile.

Typical sea breezes were simulated for the Southern Finland coast in Savijärvi & Alestalo (1988) as a function of the prevailing wind. The strongest southwesterly sea breezes (up to 11 m/s) were obtained during weak northerly large-scale winds (winds from the land), which agrees with observations. The most interesting finding was, however, that during 4-8 m/s southerly large-scale winds the then strong sea breeze of the opposite Estonian coast could be advected over the sea to

Finland, producing the curious observed, but hitherto unexplained, easterly surface winds during the late afternoon and evening.

Sea and lake breezes in the tropics were discussed in Savijärvi (1997), where special wind observations along Lake Tanganyika could be utilized to validate the model results of the complex behaviour of simultaneous lake breezes, slope winds and trade winds over that rift valley lake. The strong subtropical and tropical sea breezes were also studied in Savijärvi (1995) with a view to parameterizing their effects into large-scale models. In fact, a suggested parameterization was later tested in the ECHAM4 climate model. Although the parameterization worked well (giving extra mixing near the coastline in sea breeze conditions), its overall effect was small in a long simulation, so it was not adopted into operational use. Some other interesting but unpublished results concern the weak land breezes on the south coast of Finland (observed and modelled; a M.Sc. thesis), and coupling of the UH 1-D model version with a simple lake circulation model to study the diurnal interaction. The UH model is also used in the Finnish Institute of Marine Research by T. Vihma.

3. ONGOING MARINE *ABL* RESEARCH

At the present time we are making comparison UH model runs against Alfred Wegener Institute (AWI) aircraft flight data of the marine ABL near Spitzbergen, collected in the EU-funded Arctic Radiation and Turbulence Interaction Study (ARTIST). These excellent data are utilized to study a strong cold air outbreak from over ice to the open sea. The model reproduces the rapid warming, moistening and downstream stratocumulus cloud formation remarkably well. The observed sensible heat flux profiles are also quite well simulated, provided that the asymptotic mixing length λ is set to about 150 m. The flight observations point to a relatively weak latent heat flux with an exchange coefficient C_e much smaller than C_d or C_h. Other cases of warm outbreaks and flight observations of the arctic cloud deck will be studied next. - A cold air outbreak over the Baltic, studied in another EU project (Newbaltic), was also well simulated by the UH model, but too weak sensible heat fluxes and a too shallow mixed layer resulted from the HIRLAM (1-D version), when applied in the same case.

When testing a fully-iterative Monin-Obukhov surface layer scheme in the UH model, instead of the basic noniterative approach, the differences in the surface fluxes were minimal (below 3 %), even in the above highly unstable cold air outbreak conditions. Thus the noniterative scheme will be used as the default in future, with the slower iterative scheme as an alternative. The UH model's vertical diffusion scheme has further been tested against analytic solutions (extended Ekman spirals, Berger & Grisogono (1998)) for vertically variable K_z and V_g. The UH model reproduced the analytic steady-state wind profiles quite exactly. The radiation scheme has also been validated off-line by applying it in an AWI aircraft dataset (REFLEX-III) of stratus over the sea. The scheme was quite accurate both for the longwave and shortwave fluxes upwards and downwards through the cloud.

4. THE SURFACE LAYER IN *HIRLAM* AND IN THE *UH* MODEL OVER THE SEA

We believe, considering the above, that the key processes, including specifically the surface layer representation and vertical diffusion, are well represented in the UH model. In it, as well as in HIRLAM, the surface drag coefficient C_d is given by $C_d = C_{dn} \cdot f_m(Ri)$ where the neutral drag coefficient is $C_{dn} = (k/\ln(z_a/z_{om}))^2$. Here k is von Kármán constant (0.4), z_a is the reference height (model's lowest level), z_{om} the surface roughness length for momentum, and f_m includes all stability effects for momentum with the bulk Richardson number Ri as the measure of stability. Similar forms are defined for C_h, with z_{om}, z_{oh} and $f_m(Ri)$, $f_h(Ri)$ to be determined from field observations. C_e is equated to C_h in both HIRLAM and the UH model. Above the lowest (i.e. surface) layer, vertical diffusivity is given in both models via $K_m = l^2 |\partial V/\partial z| \cdot f_m(Ri)$, $K_h = l^2 |\partial V/\partial z| \cdot f_h(Ri)$, with the "Blackadar" formulation for the mixing length $l = l(z,\lambda)$, so differences may arise from definitions of the roughness lengths and/or stability functions.

In a recent study, Zeng & al. (1998) utilized large observational ship datasets to estimate z_{om} and C_{dn} over the ocean. They concluded that formally $z_{om} = 0.013 \cdot (u_f)^2/g + 1.65 \cdot 10^{-6}/u_f$, where u_f is the friction velocity. The constant value $z_{om} = 0.1$ mm used in the UH model over ocean was in the middle of their (broad) cloud of retrieved z_{om} values for all wind speeds up to 18 m/s. HIRLAM uses the original Charnock's formula $z_{om} = 0.018 \cdot (u_f)^2/g$, so its neutral sea roughness could be slightly on the high side, especially for the limited fetches common in the Baltic Sea.

In the unstable case, the UH scheme is based on the Dyer-Businger forms of the universal stability functions $\phi_m(z/L)$, $\phi_h(z/L)$. These lead to $f_m = (1 - 15 \cdot Ri)^{1/2}$, $f_h = (1 - 15 \cdot Ri)^{3/4}$. The results with these f(Ri) used by the UH model verify well against observations and iterative M-O calculations, as stated in Section 3. The HIRLAM 2.5 (Louis) scheme defines the stability functions f_m, f_h differently; values now also depend strongly on z_a/z_o (unlike the UH scheme). In Table 1, numerical values of f_m and f_h in the UH model and HIRLAM are compared for some Ri, using $z_a = 10$ m, and $z_{om} = z_{oh} = 0.1$ mm, typical for a sea surface. The HIRLAM formulas have been coded directly from the HIRLAM Documentation Manual.

Table 1. The stability functions f_m, f_h from HIRLAM and from the UH model for unstable Ri values over smooth surface (sea; $z_a/z_o = 10^5$).

Ri	f_m (UH)	f_m (HIRLAM)	f_h (UH)	f_h (HIRLAM)
0	1.	1.	1.	1.
-0.1	1.581	1.209	1.988	1.321
-0.2	2.000	1.311	2.828	1.482
-0.3	2.345	1.392	3.591	1.612
-0.4	2.646	1.463	4.304	1.727
-0.5	2.915	1.526	4.978	1.831
-0.6	3.162	1.585	5.623	1.927
-0.7	3.391	1.640	6.245	2.019
-0.8	3.606	1.692	6.846	2.105
-0.9	3.808	1.741	7.431	2.189
-1.0	4.000	1.789	8.000	2.269

It is seen from Table 1 that for the marine ABL in unstable conditions, the HIRLAM scheme may tend to underestimate flux transfers between sea and air. For instance, at Ri = -0.5, the UH scheme increases C_h and hence the sensible and latent heat fluxes by a factor of 5 over their neutral values, but HIRLAM by less than 2. As the same stability functions are also used higher up in the respective vertical diffusion schemes, this might explain the low sensible and latent heat fluxes and shallow mixed layers in unstable conditions over the sea produced by HIRLAM (e.g. in the cold air outbreak case discussed in Section 3). For rougher surfaces typical over land, the UH and HIRLAM values for f_m, f_h are, however, closer to each other.

In the stable boundary layer, the scatter in the observational measurement points for the determination of ϕ_m, ϕ_h (and f_m, f_h) is typically quite wide. The UH model uses a simple formula, $f_m = f_h = \max(0.1, 1\text{-}5 \cdot Ri)$. The linear decay of f_m with increasing Ri for slightly stable conditions is supported by e.g. the Wangara experiment data, and the adopted UH formula preserves turbulence at a 10 % "background" level of its neutral values in very stable conditions (Ri > 0.2). Recent careful measurements and analysis by Mahrt & al. (1998) also tends to support both of these aspects. In Table 2 the UH values of $f_m(Ri)$, Ri > 0, are compared with the Dyer-Businger-derived, and HIRLAM values. The latter does not depend anymore on z_a/z_o in stable conditions. It produces, however, more drag than the UH or D-B formulae in very stable conditions (thus allowing for too much drag and background turbulence?), but slightly less than the UH scheme in slightly unstable conditions. The same also applies for the f_h formulation of HIRLAM.

In conclusion, in the typical slightly stable conditions over the sea, HIRLAM might slightly underestimate surface fluxes due to the formulation of its f_m, f_h, but the slightly high values of z_{om}, z_{oh} over the sea tend to compensate this. In unstable conditions, however, the then quite strong underestimation of f(Ri) (compared to the UH model and Dyer-Businger formulae) might be a problem over the sea (and over other smooth surfaces with $z_a/z_o > 10^4$), but not so much over the rough land. This makes the possible problem difficult to discover from observations, which are usually scarce and inaccurate over the sea.

Table 2. The stability functions f_m, f_h from HIRLAM and from the UH model, and f_m from the Dyer-Businger universal functions (D-B) for some stable Ri values.

Ri	$f_m = f_h$ (UH)	f_m (D-B)	f_m (HIRLAM)	f_h (HIRLAM)
0.02	0.9	0.81	0.840	0.761
0.04	0.8	0.64	0.733	0.603
0.06	0.7	0.49	0.655	0.494
0.08	0.6	0.36	0.597	0.413
0.10	0.5	0.25	0.551	0.352
0.12	0.4	0.16	0.513	0.305
0.14	0.3	0.09	0.482	0.268
0.16	0.2	0.04	0.456	0.237
0.18	0.1	0.01	0.434	0.212
0.20	0.1	0	0.414	0.191
0.22	0.1	0	0.397	0.173

REFERENCES

Alestalo, M. & Savijärvi, H. 1985: Mesoscale circulations in a hydrostatic model: Coastal convergence and orographic lifting. - Tellus, 37A:156-162.

Berger, B.W. & Grisogono, B. 1998: The baroclinic, variable eddy viscosity Ekman layer. - Boundary-Layer Meteor., 87:363-380.

Mahrt, L., Sun, J., Blumen, W., Delany, T. & Oncley, S. 1998: Nocturnal boundary layer regimes. - Boundary-Layer Meteor., 88:255-278.

Neumann, J. & Savijärvi, H. 1986: The sea breeze on a steep coast. - Beitr. Phys. Atmos., 59:375-389.

Savijärvi, H. 1985: The sea breeze and urban heat island in a numerical model. - Geophysica, 21, No. 2, 115-126.

Savijärvi, H. & Alestalo, M. 1988: The sea breeze over a lake or gulf as the function of the prevailing flow. - Beitr. Phys. Atmos., 61:98-104.

Savijärvi, H. 1995: Sea breeze effects on large-scale atmospheric flow. - Contr. Atmos. Phys., 68:335-344.

Savijärvi, H. 1997: Diurnal winds around Lake Tanganyika. - Quart. J. Roy. Meteor. Soc., 123:901-918.

Savijärvi, H. 1999: A model study of the atmospheric boundary layer in the Mars Pathfinder lander conditions. - Quart. J. Roy. Meteor. Soc., 125:483-493.

Zeng, X., Zhao, M. & Dickinson, R.E. 1998: Intercomparison of bulk aerodynamic algorithms for the computation of sea surface fluxes using TOGA, COARE and TAO data. - J. Clim., 11:2628-2644.

AIR-ICE COUPLING AND THERMODYNAMIC MODELLING OF SEA ICE

Jouko Launiainen, Cheng Bin, Juha Uotila & Timo Vihma

Finnish Institute of Marine Research
Box 33, FIN-00931 Helsinki, Finland

1. INTRODUCTION

Air-ice-ocean coupling is an important task in marine meteorological modelling and forecasting. In the air-ice coupling, the primary quantities to be studied include air-ice interfacial (surface) temperature, momentum, heat, and water vapour (latent heat) fluxes, and radiative fluxes. In this report, the Finnish Institute of Marine Research (FIMR) experimental process studies and modelling studies into air-ice-ocean coupling are introduced.

2. COUPLED MODEL

For local process air-ice-ocean studies, a one-dimensional coupled thermodynamic air-ice-ocean model (Launiainen & Cheng, 1998) was constructed. A schematic presentation of the model is given in Fig. 1.

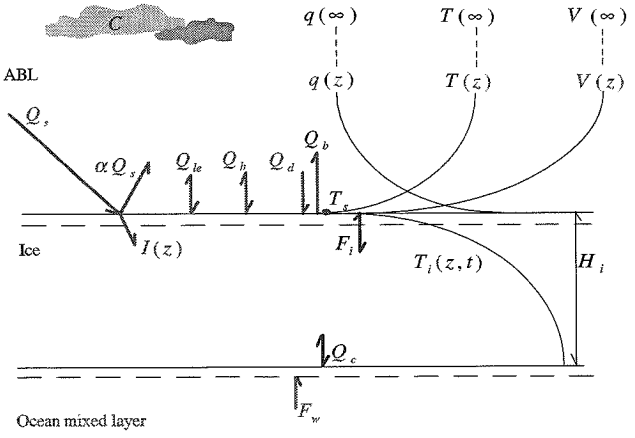

In:

ABL

Short-wave (Q_s, I) and long-wave (Q_d, Q_b) rad. fluxes

Turbulent fluxes of momentum, sensible heat (Q_h) and latent heat (Q_{le})

Monin-Obukhov similarity defined profiles

Surface heat balance and T_s *to be controlled by it*

ICE

Heat conduction (F_i) in snow and ice
Short-wave penetration ($q(z,t)$) in snow and ice

OBL

Heat flux (F_w) from ocean

Fig. 1. Coupled FIMR 1D thermodynamic Air-Ice-Ocean Model.

In total, the ice model has 10 to 30 layers in snow and ice, and the time step may be from 10 s upwards. Air and snow/ice are fully coupled in each time step calculation. The input data are as follows: wind speed, temperature and moisture from any level (arbitrary and mutually different, if necessary) in the constant flux layer, say below 50 m, and short-wave radiation. If radiation data are not available, these will be calculated by standard formulae in the model. In addition, initial ice and snow thicknesses are given. The output data are as follows:

- Air-ice fluxes and atmospheric stratification.
- Atmospheric profiles of wind, temperature and humidity. The model can e.g. produce a surface layer inversion under conditions of negative surface radiation balance.
- Ice thickness and in-ice temperature at various depths in the ice.

As a module, the ice model has been coupled with a mesoscale atmospheric model.

Fig. 2 gives an example of a model application. The model-estimated vertical temperature of air and in-ice temperatures are given. The atmospheric temperature profiles indicate an interesting inversion, in the case selected.

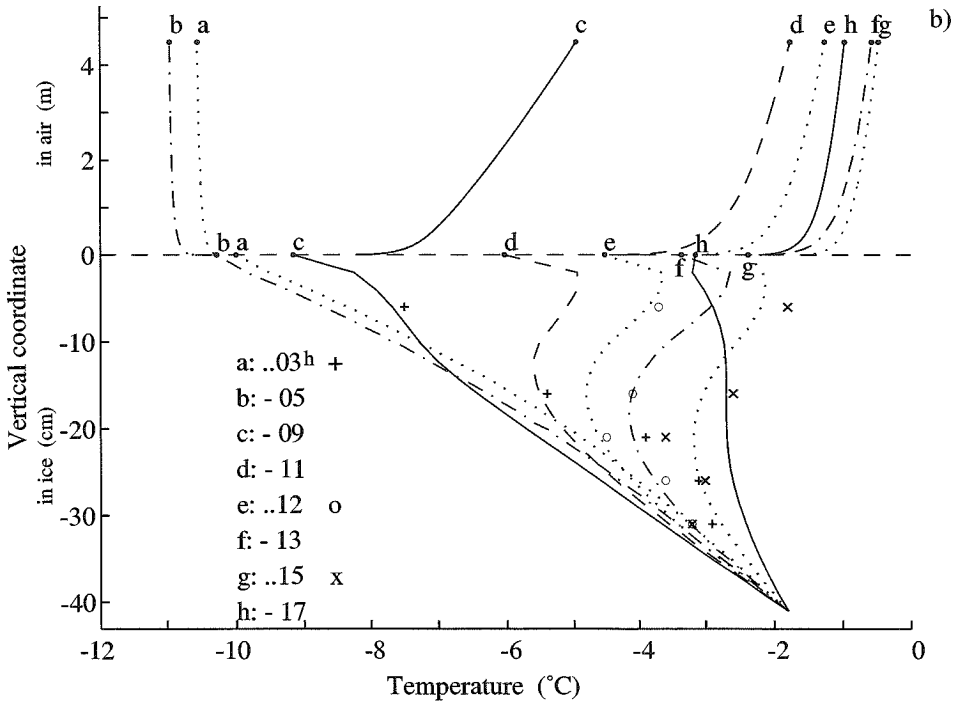

Fig. 2. Vertical profiles of air temperature and in-ice temperature, corresponding to various times on 31 January, 1990, during the Bohai Sea (China) case study. The graphs give the estimates by the coupled model. A few in-ice temperature observations available are given as point symbols. Note the different vertical scaling in air and in ice. (From Launiainen & Cheng, 1998, Fig. 9b).

3. EXPERIMENTAL STUDIES

The FIMR is coordinating the Baltic Air-Sea-Ice Study (BASIS) which is a sub-project of GEWEX/BALTEX. The overall objective of BASIS is *to create and analyse an experimental data set for optimization and verification of coupled atmosphere-ice-ocean models.* BASIS is carried out as an EC-funded project by Finnish, Swedish and German institutes. The main experimental campaign was carried out in the northern Baltic Sea, in February-March 1998. In the network, data were collected by research vessels, aircraft and helicopters, drifters and automatic stations, and by meteorological sounding stations.

The FIMR air-ice-sea process study measurements included direct eddy flux (sonic anemometer) measurements, and wind and temperature measurements on a meteorological profile mast on the sea ice. In addition, various radiation fluxes were measured and in-ice/snow temperature measurements were collected using an ice temperature logging stick. Finally, water-ice fluxes of heat, momentum and salt were measured (by the University of Hokkaido, Japan) with various eddy flux equipment below the ice. The observations are introduced in the BASIS Data Report (Launiainen, 1999).

The wind and temperature measurements allowed us to calculate the fluxes of momentum and sensible heat for comparison with the eddy-flux observed results, using the so-called gradient (level difference) method based on the Monin-Obukhov similarity theory. The results from the sensible heat flux measurements are given in Fig. 3. With the wind and temperature sensors especially calibrated, the level difference and the eddy flux results were well compatible. As a third,

practically independent, method, the air-ice fluxes were calculated with the coupled model described above, and the results were (Fig. 3) comparable with those of the eddy-flux and level difference method. The results are encouraging, and justify the overall construction of the coupled model.

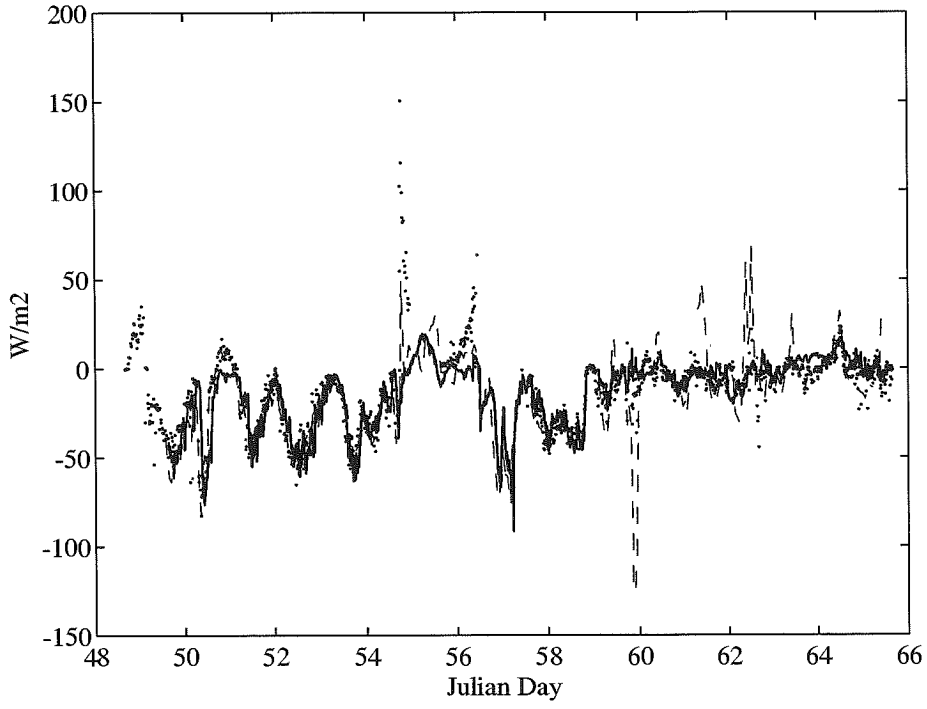

Fig. 3. Sensible heat flux at Aranda Ice Station during BASIS as measured by the sonic anemometer (dotted; 10 min values), calculated by the level-difference profile method (broken; hourly means) and, calculated by the coupled air-ice-ocean model (continuous; 10 min values). Upward flux positive.

As an example of the air-ice interaction characteristics, Fig. 4 gives the neutral drag coefficient $C_{DN}(10)$ as a function of the wind speed, as calculated from the sonic anemometer data from the Ice Station. The results show a drag coefficient of 1.2 x 10^{-3} in those conditions over rather smooth sea ice at the Aranda Ice Station during BASIS-98.

Finally, we may note that the above discussion is strictly related to a local one-dimensional approach. In nature, a sea ice field usually consists of a mosaic of open water and ice floes of various thickness, and the field is therefore heterogeneous with respect to the surface temperature and roughness. Spatial averaging is therefore necessary to estimate regionally-representative air-sea-ice fluxes, and several possibilities are available for the parameterization of them (Vihma, 1995). For this purpose, the FIMR thermodynamic model is coupled as a module to a mesoscale atmosphere model.

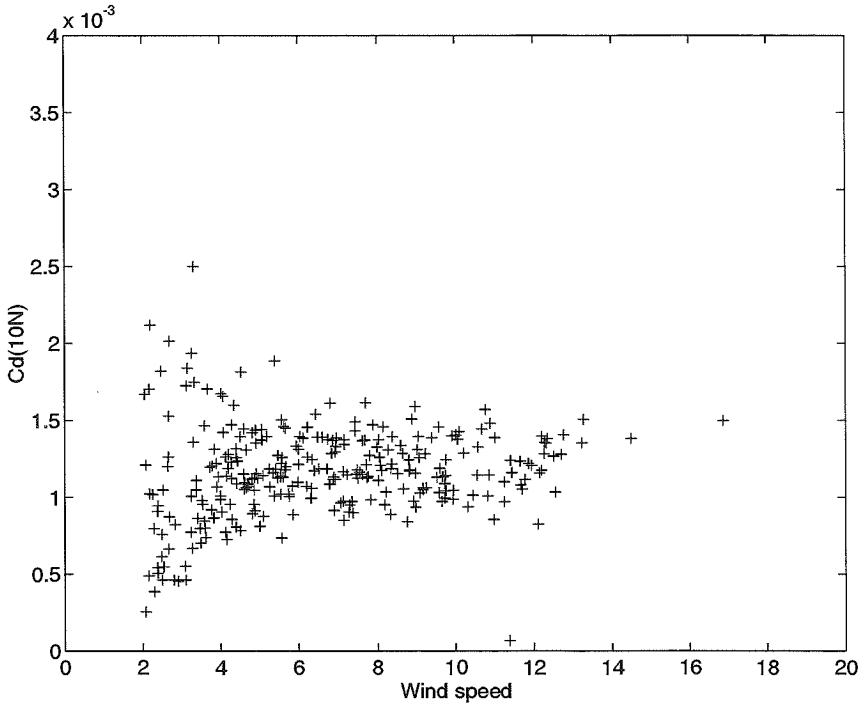

Fig. 4. Drag coefficient $C_{DN}(10)$ derived from the eddy-flux measurements as a function of wind speed at the Aranda Ice Station in BASIS-98.

REFERENCES

Launiainen, J. & Cheng, B. 1998: Modelling of ice thermodynamics in natural water bodies. - Cold regions science and technology 27:153-178.

Launiainen, J. (Ed.), 1999: BALTEX-BASIS, BASIS-98 Data Report. - International BALTEX Secretariat, Publication No. 14, 92 pp.

Vihma, T. 1995: Subgrid parameterization of surface heat and momentum fluxes over polar oceans. - J. Geophys. Res., 100, 22,625-22,646.

OBSERVATIONS AND MODELLING OF THE ATMOSPHERIC BOUNDARY LAYER OVER SEA ICE

Timo Vihma, Juha Uotila & Jouko Launiainen

Finnish Institute of Marine Research, P.O. Box 33, FIN-00931 Helsinki, Finland

ABSTRACT

Observations of the atmospheric boundary layer (ABL) over sea ice are presented from the Baltic Sea, the Weddell Sea, and the Denmark Strait. In all these regions the ABL was characterised by the frequent presence of temperature inversions and low-level jets. The summer inversions over the Weddell Sea and Denmark Strait resembled the winter inversions over the ice edge zone in the Baltic Sea. The formation of low-level jets via two mechanisms, baroclinity and undamped inertial oscillations, was studied by data analyses and modelling, and, in particular, the baroclinic mechanism seems to be important during ice-parallel flow.

1. INTRODUCTION

The atmospheric boundary layer (ABL) over sea ice is characterised by certain properties, which make it differ from the ABL over continents and the open ocean. These properties result from the nature of the sea ice surface. First of all, the surface tends to be non-stationary, and the surface temperature and roughness over a given point can change rapidly due to ice deformation or advection, and less rapidly due to thermodynamic ice formation, snowfall, or ice or snow melt. Surface roughness also changes due to ice ridging. Compared to land surfaces, the sea ice cover is relatively homogeneous with respect to roughness, although the ice freeboard, ridges, and sastrugi cause form drag, which adds to the skin friction and has an uneven spatial distribution. By contrast, during cold weather the sea covered by a broken ice field is extremely inhomogeneous with respect to its surface temperature. The ice surface and the near-surface air may have temperatures down to -30°C, while open leads simultaneously remain at the freezing point of about -1.8°C (about -0.3°C in the Baltic Sea).

The ice cover typically has a negative radiation balance, resulting in a stable stratification and a temperature inversion. A stably-stratified surface layer is also often caused by advection of warm air from the open sea. Over leads the stratification is typically strongly unstable, and heat plumes rise from the open water. Internal boundary layers (IBLs) are therefore developed. In cases of narrow and frequent leads the IBLs typically merge at a so-called blending height, and the ABL above the blending height feels the spatially-integrated effects of the fractured surface. Heat plumes from leads may, however, occasionally penetrate through the Arctic inversion and reach a height of a few kilometres (Schnell & al., 1989).

On a local scale, an edge between the sea ice and the open water causes a step-change for the forcing of the ABL. On a global scale, the inner ice pack is typically separated from the open ocean by the marginal ice zone (MIZ), which often appears as a diffuse mixture of ice and water. Via a spatial change in the surface fluxes, the ice edge zone causes baroclinity in the lower atmosphere, which is often seen in the wind field too (Guest & al., 1995).

2. OBSERVATIONS

A summary of our observations on the ABL over sea ice during the 1990s is presented in Table 1. The field experiments are described in Launiainen & Vihma (1994), Uotila & al. (1997), and Vihma & al. (1996, 1998, 1999). In addition to the observations listed in Table 1, in 1998 a joint European program BALTEX-BASIS (Launiainen, 1999) included multidisciplinary observations

by Swedish and German groups over and around the Gulf of Bothnia. We also participated in the field phase of the Arctic Radiation and Turbulence Interaction Study (ARTIST, Hartmann & al., 1999), in which our contribution is mostly in the modelling.

Table 1. Expedition years and observation types in various regions.

Observations	Weddell Sea	Denmark Strait	Baltic Sea
Ship weather station[+]	1990, 1992, 1996	1993, 1997	1994, 1995, 1997, 1998
Rawinsonde soundings	1990, 1996	1993	1994, 1995, 1997, 1998
Meteorological buoys	1990-91, 1992, 1996-97		1998
Radiation components*	1996		1994, 1997, 1998
Turbulence[⊥]	1996		1997, 1998
Profile mast^			1994, 1997, 1998

[+]Sensors for atmospheric pressure, air temperature and humidity, wind speed and direction, and downward shortwave radiation. Two sensors for each quantity, except the pressure, on both sides of the ship.

*Downward and reflected shortwave radiation, upward longwave radiation and the net radiation at the surface

[⊥]Measured by a sonic anemometer two metres above the surface

^Wind speed measured at five levels, air temperature at three levels, and air humidity and wind direction at a single level.

3. TEMPERATURE INVERSIONS

A temperature inversion is a typical feature over sea ice. The properties of inversions can be characterised by the inversion base height, thickness of the inversion layer, base temperature, and inversion strength (difference between the top and base temperatures). Over central Arctic and Antarctic sea ice in winter, the inversions are typically surface-based, reaching a height of about 1200 m, and having a strength of 10-12°C (Serreze & al., 1992; Claffey & al., 1994). A summary of the inversion properties in our observations is presented in Figure 1. For reference, we also present observations over the open ocean in the Weddell Sea (summer) and Baltic Sea (spring). We see that the inversions were elevated, with the base being high, particularly in the Weddell Sea, both over the open ocean, but also over the MIZ. The latter effect was most probably due to the heating from the open parts of the fractured ice cover. The inversions over the open Baltic Sea in May were practically surface-based (the lowest 20 m were disturbed by the ship), and refer to spring conditions with the sea much colder than the surrounding continent. The thickness of the inversions was typically 100-300 m, which is much less than that of the polar winter inversions. The inversion strengths were typically 1-4°C, the strongest ones occurring in the Denmark Strait MIZ. Thus, all the inversions we observed were weak compared to the polar winter cases. Also, the base temperatures were more than 10°C higher than those over the polar sea ice in winter. We note that the inversions in the Baltic Sea in winter were approximately comparable to those over the polar oceans in summer. However, our observations from the wintertime Baltic Sea were from a region close to the ice edge.

4. LOW-LEVEL JETS: OBSERVATIONS AND MODELLING

We define a low-level jet as a local maximum in the wind profile that is at least 2 m/s higher than the speeds both above and below it. A low-level jet is a typical feature over a stably stratified surface, and can be characterised by the jet core height and jet strength (ratio of the jet core wind speed to the wind speed minimum just above the jet). A summary of our observations is presented in Figure 1. We see that the jet core heights are around 400-600 m, except over the open Weddell Sea. In the Baltic Sea and the Denmark Strait the jets were typically above the inversion layers, while in the Weddell Sea the jets were below the inversions. The median values for the jet core wind speeds were 8-13 m/s, and the jet strengths were 1.6-2.4.

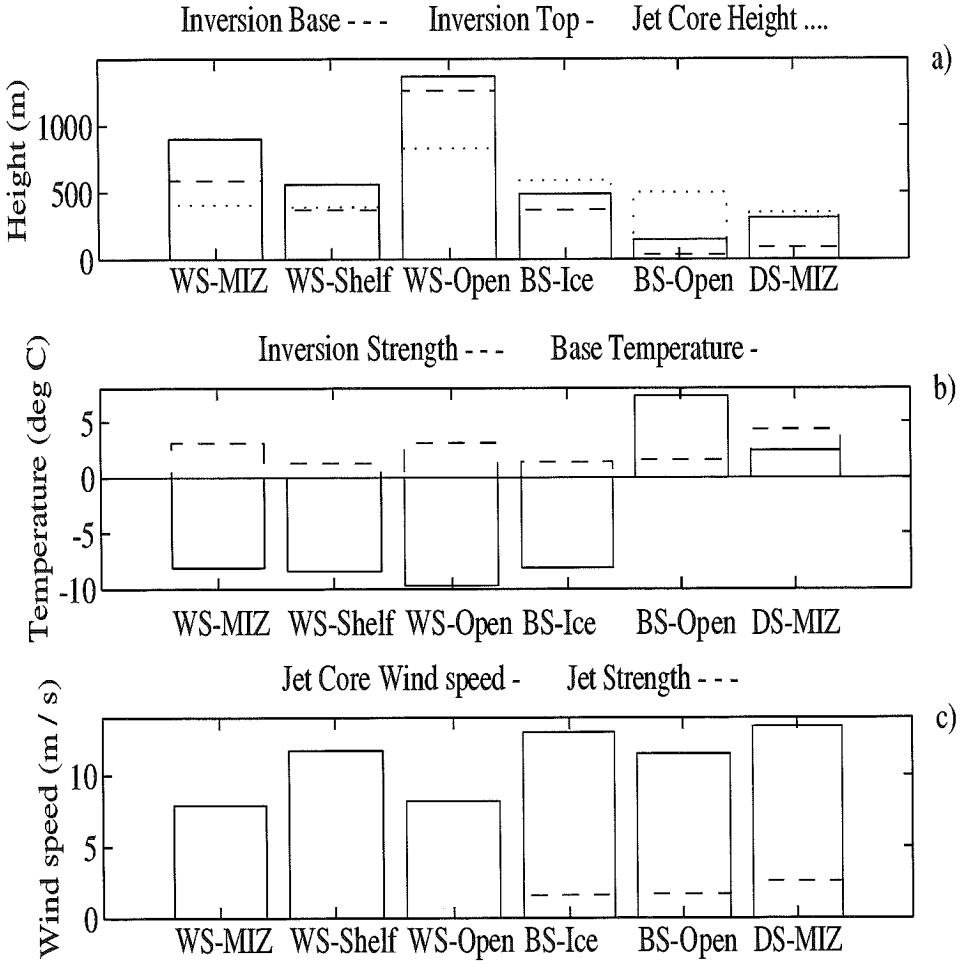

Fig. 1. Median values for (a) the inversion base (dashed line), inversion top (solid line), and the jet core height (dotted line); (b) the inversion strength (dashed line) and base temperature (solid line); (c) the jet core wind speed (solid line) and jet strength (dashed line). The results are for the Weddell Sea MIZ (WS-MIZ) in summer, the Weddell Sea at the edge of the floating continental ice shelf (WS-Shelf), the open ocean in the Weddell Sea (WS-Open), the ice-covered Baltic Sea (BS-Ice), the open Baltic Sea (BS-Open), and the Denmark Strait MIZ (DS-MIZ).

Various physical mechanisms may generate a low-level jet. Baroclinity has its most pronounced effect for flow parallel with the surface temperature front (e.g. ice edge) with the cold surface on the right of the wind (looking, in the northern hemisphere, in the direction the wind is blowing towards); the thermal wind then opposes the wind direction. In the resulting wind profile, the thermal wind reduces the wind speed above the jet core while friction reduces the wind below the jet core. This mechanism was suspected as being the reason for the pronounced low-level jets in the Denmark Strait in conditions with the wind from the north-east (Vihma & al., 1998).

An attempt to model the baroclinic effect was made using a two-dimensional hydrostatic mesoscale ABL model (Alestalo & Savijärvi, 1985). The model domain consisted of 60 km of ice and 60 km of open ocean surface, the flow being forced by a geostrophic wind of 10 m/s parallel to the ice edge. The initial surface temperature was -20°C over the ice and -1.8°C over the open ocean, and the initial lapse rate was -1 K/km. The steady-state wind field is shown in Figure 2a. We see a wind maximum of 12 m/s at a height of 150 m over the ice edge, and reduced winds above it. When the simulation was repeated with the geostrophic wind turned through 180°, the jet was absent.

Aircraft measurements of the ABL over the ice edge zone provide a sample (along the flight pattern) of the conditions in the study area. One objective of the ARTIST project is to develop a method for optimising the aircraft measurements: an optimal flight pattern minimises the unexplained variance in the quantity of interest, between the whole study area and the sample. Figure 2b represents an aircraft flight pattern that minimises the unexplained variance in the wind speed in the situation of Figure 2a. The practical restrictions inherent in the aircraft flight capability were taken into account while calculating the pattern.

Observations of low-level jets over an ice surface may also result from undamped inertial oscillations, which form a jet that is analogous in space to the classical nocturnal jet (advection of warm air over a cold ice surface is a spatial analogy to sunset over a land surface.) The effect of inertial oscillations was studied by simulating an on-ice flow with warm air temperatures. Simulations were made with model versions having 10-50 levels in the vertical. The effect of inertial oscillations on the formation of low-level jets did not became very apparent. A small jet could often be detected in the wind profile, but the jet core wind speed did not exceed the geostrophic wind speed by more than 20 %. An example is given in Figure 3 (the 2 m/s criterion is, in fact, not fulfilled). The jet at the height of 70 m is most pronounced at a distance of 70 km from the ice edge, corresponding to a travel time of 3.8 h, which is 1/3 of the inertial period at a latitude of 78°N. After a whole inertial period of 12.3 h (corresponding to a distance of 200 km), the wind profile has almost returned to its original state at the ice edge. The model results are close to the observations of Andreas & al. (1995) in the Weddell Sea.

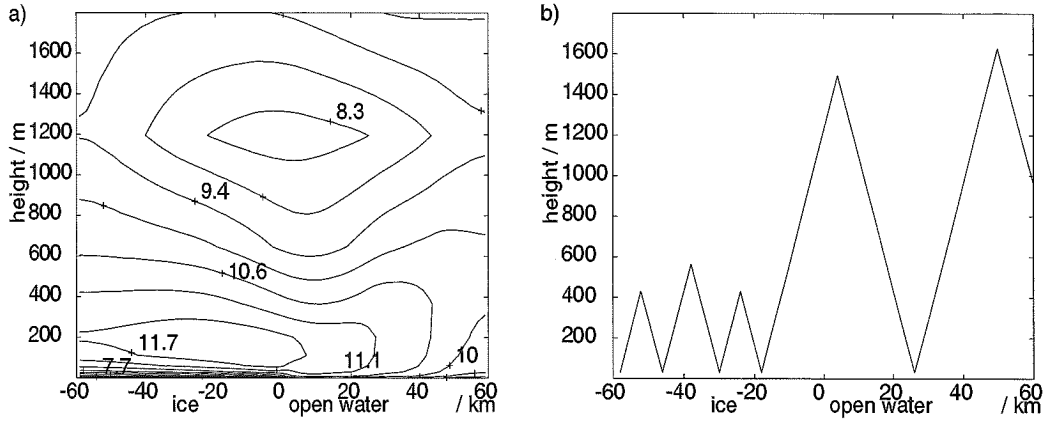

Fig. 2. (a) Cross-section of the wind speed over a 120 km wide region, centred at the ice edge, and (b) the optimal flight pattern to minimise the unexplained variance in the wind speed. The geostrophic wind is parallel to the ice edge ("out of the page") with a speed of 10 m/s.

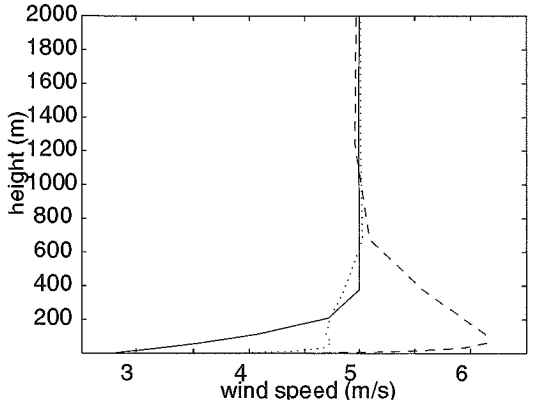

Fig. 3. Wind profiles at the ice edge (continuous line), 70 km downwind (broken line), and 200 km downwind (dotted line) over the ice in a case of warm air (near-surface temperature 0°C) advection over the cold ice surface.

Acknowledgements

The work has been supported by the European Commission through contracts MAST3-CT97-0117 and ENV4-CT97-0487.

REFERENCES

Alestalo, M., & Savijärvi, H. 1985: Mesoscale circulations in a hydrostatic model: coastal convergence and orographic lifting. - Tellus, Ser. A, 37A, 156-162.

Claffey, K.J., Andreas, E.L. & Makshtas, A.P. 1994: upper-air data collected on ice station Weddell. - Spec. rep. 94-25, 68 pp., U.S. Army Cold Reg. Res. and Eng. Lab., Hanover, N.H.

Guest, P.S., Glendening, J.W. & Davidson, K.L. 1995: An observational and numerical study of wind stress variations within marginal ice zones. - J. Geophys. Res., 100, 10,887-10,904.

Hartmann, J., Albers, F., Argentini, S., Bochert, A., Bonafe, U., Cohrs, W., Conidi, A., Freese, D., Georgiadis, T., Ippoliti, A., Kaleschke, L., Lupkes, C., Maixner, U., Mastrantonio, G., Ravegnani, F., Reuter, A., Trivellone, G. & Viola, A. 1999: Arctic Radiation and Turbulence Interaction study. - Rep. Polar Res. No. 305, Alfred Wegener Institute for Polar and Marine Res., Bremerhaven, 87 p.

Launiainen, J. (Editor), 1999: BALTEX-BASIS Data Report 1998. - International BALTEX Secretariat Publication No 14, 94 p.

Launiainen, J. & Vihma, T. 1994: On the surface heat fluxes in the Weddell Sea. - In: The Polar Oceans and Their Role in Shaping the Global Environment, Nansen Centennial Volume, edited by O.M. Johannessen, R. Muench & J.E. Overland. - Geophysical Monograph Series, 85, American Geophysical Union, pp. 399-419.

Schnell, R.C., Barry, R.G., Miles, M.W., Andreas, E.L., Radke, L.F., Brock, C.A., McCormick, M.P. & Moore, J.L. 1989: Lidar detection of leads in Arctic sea ice. - Nature, 339, 530-532.

Serreze, M.C., Kahl, J.D. & Schnell, R.C. 1992: Low-level temperature inversions of the Eurasian Arctic and comparisons with Soviet drifting station data. - J. Clim., 5, 599-613.

Uotila, J., Vihma, T. & Launiainen, J. 1997: Marine meteorological radiosoundings in the northern Baltic Sea from R/V Aranda in 1994-95. - Meri, Report Series of The Finnish Institute of Marine Research, no. 30, 57 p.

Vihma, T., Launiainen, J. & Uotila, J. 1996: Weddell Sea ice drift: kinematics and wind forcing. - J. Geophys. Res. 101:18279-18296.

Vihma, T., Uotila, J. & Launiainen, J. 1998: Air-sea interaction over a thermal marine front in the Denmark Strait. - J. Geophys. Res., 103, 27,665-27,678.

Vihma, T., Uotila, J. & Launiainen, J. 1999: Surface heat balance in the Weddell Sea: Buoy observations and comparisons with large-scale models. - submitted to J. Geophys. Res.

MODELLING OF THE BALTIC SEA ICE THICKNESS DISTRIBUTION

Jari Haapala

Department of Geophysics
P.O. Box 4 (Fabianinkatu 24 A), FIN-00014 University of Helsinki, Finland

ABSTRACT

Pack ice is a mixture of several ice types and open water. Each ice type has its own characteristic thickness, temperature, roughness etc., and has a specific effect on the ice dynamics, as well as on the heat and momentum exchange between the atmosphere and the ocean. Present ice models resolve the amount of open water and the mean ice thickness, and distinguish ridged ice from level ice. That approach has been extended, and a new ice thickness redistribution model has been formulated, in which the pack ice is decomposed into open water, two different type of undeformed ice, and rafted, rubble and ridged ice. The ice thickness distribution model has been included in a coupled ice-ocean model, and numerical experiments have been made for the simulation of the Baltic Sea ice season. The benefits of the extended ice classification are a separation of the thermally and mechanically produced ice and a better description of the minimum ice strength. The different thermodynamic growth/melting rates of the various ice types can also be introduced into the model, hence giving a more detailed seasonal evolution of the pack ice. In addition, the six-level ice thickness distribution model gives more information about the surface properties (surface temperature, albedo, roughness) of the pack ice.

INTRODUCTION

Sea ice is composed of open water, undeformed ice and deformed ice. Undeformed ice is produced by the thermodynamic growth of sea ice as a result of the freezing of sea water. The dynamics of the ice pack is responsible for the production of deformed ice. During convergent ice motion, ice floes are compressed together, forming rafted, rubble and ridged ice - deformed ice in general. The proportion of mechanically-produced ice has been estimated as being about 1/3 of the total ice mass in the Baltic (Lewis & al., 1993) and 1/3 to 2/3 in the Arctic (Flato & Hibler, 1995).

The modelling of ice thickness redistribution is an essential research topic in sea ice modelling, because the physical behaviour of sea ice is highly dependent on the ice thickness characteristics. Generally, it is known that the ice velocity field depends on the ice thickness distribution and vice versa, and previous model studies (Leppäranta & al., 1998) suggest a better description of ice thickness for improving the dynamic ice model simulation. Also, properties of ice, such as ice thickness, strength, albedo, and roughness are dependent on the ice type. These properties may vary very much between ice types, and a detailed description of the ice surface characteristics is necessary for coupled models for the calculation of realistic fluxes of heat and momentum at the ocean-ice-atmosphere interface.

Present ice models do not produce answers as to when, where and how much deformed ice is generated on a seasonal scale. The only exception is the Flato & Hibler (1994) model, which solves the ice thickness distribution function (Thorndike & al., 1975) separately for the undeformed and deformed ice. An alternative approach based on the physical ice classes has been developed. The Gray & Killworth (1996) evolution equations for the ice concentration and thickness have been extended, and a new ice thickness redistribution model has been formulated, in which the pack ice is decomposed into open water, two different type of undeformed ice, and rafted ice, rubble ice and ridged ice. The ice thickness distribution model has been included in a coupled ice-ocean model (Haapala & Leppäranta, 1996) and numerical experiments have been made for the winter of 1994. The simulation period began on 1 May 1993 and the model was run until the final ice

disappearance. Thus the model calculates the warming of the ocean surface layer during the summer season, the cooling during the autumn period, the initial freezing of sea water and the whole evolution of the ice pack during the winter months. A detailed description of the model and an analysis of the numerical experiments are given in Haapala (1999).

RESULTS

Benefits of the physically-based ice thickness distribution model include the facts that the ice classes are prognostic variables and the specific thermodynamic growth/decay is calculated for each ice class. The main advance of the model is the separation of the thermally and mechanically produced ice.

The numerical experiment for the Baltic Sea has shown that the model produced a realistic seasonal evolution of the pack ice. Most of the deformation is produced at the coastal zone during stormy periods. The coastal zone is also an important source of thermodynamically-produced ice because of the ice growth in leads. The modelled maximum mechanical growth rate of ice was 3-5 cm/day which was about the same as the maximum thermodynamical ice production rate. The deformed ice fraction was 1/3 of the total ice mass during mid-winter, and the fraction increased up to 100 % during the spring period (Fig. 1).

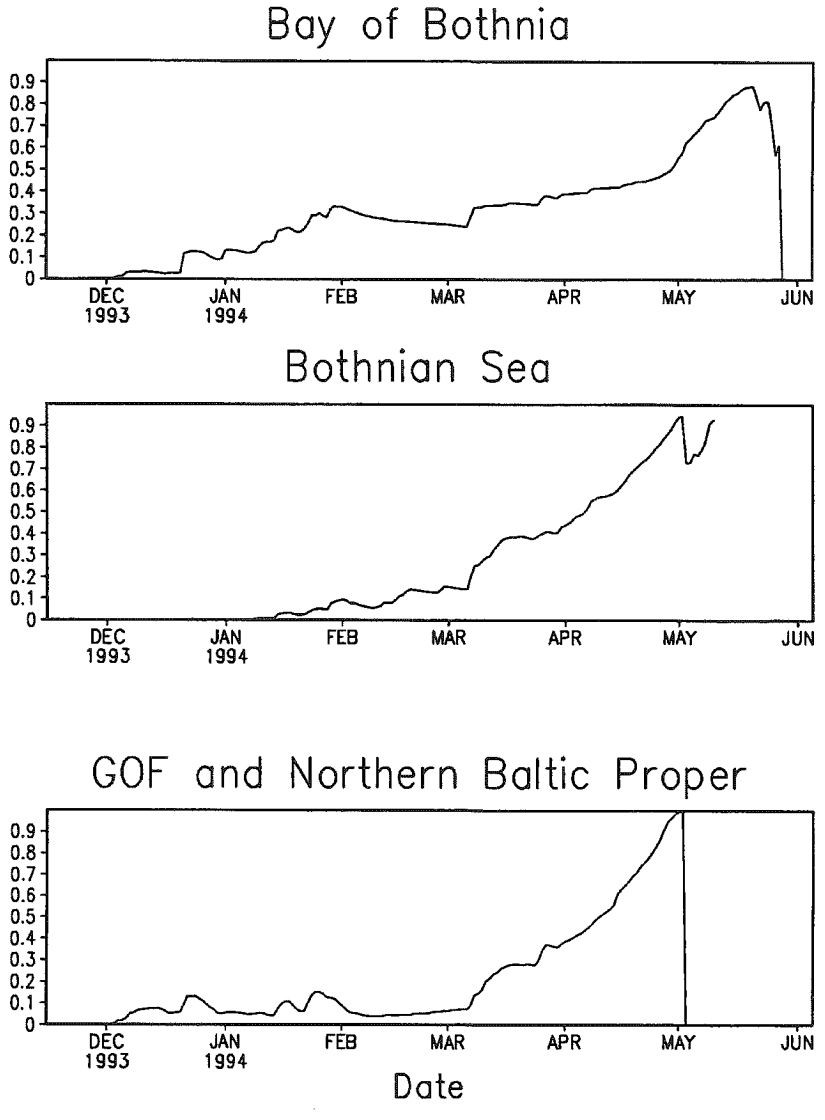

Fig. 1. Modelled deformed ice portion of the total ice mass in the Baltic sub-basins during winter 1994.

The ice class approach gives more information on the surface properties of the ice pack than the widely-used 2-level model of Hibler (1979) and its recent developments (Harder & Lemke, 1994). Ice concentration, surface temperature, albedo and surface roughness are the primary factors governing the atmospheric and oceanic boundary layers, and since these parameters are explicitly resolved for each ice class, a detailed calculation of the exchange of heat and momentum between the atmosphere/ice/ocean interface is made possible.

In the near future it will be possible to utilize remote sensing and model data for sea ice research considerably more deeply, since remote-sensing ice classification algorithms are also capable of resolving ice classes. Hence, remote-sensing data can be used for the verification of the redistribution functions and even for the assimilation into the ice model.

Acknowledgements

This work was supported by the Baltic Sea System Study of the European Commission Marine Science and Technology program MAST III, under contract MAS3-CT96-0058.

REFERENCES

Flato, G.M. & Hibler III, W.D. 1995: Ridging and strength in the modelling the thickness distribution of Arctic sea ice. - J. Geophys. Res, 100(C9), 18 611-18 626.

Gray, J.M.N.T. & Killworth, P.D. 1996: Sea ice ridging schemes. - J. Phys. Oceangr., 26, 2420-2428.

Haapala, J. 1999: Modelling of the ice thickness redistribution. (Manuscript)

Haapala, J. & Leppäranta, M. 1996: Simulating the Baltic Sea ice season with a coupled ice-ocean model. - Tellus, 48A, 622-643.

Harder, M. & Lemke, P. 1994: Modelling the extent of sea ice ridging in the Weddell Sea. - The Polar Oceans and Their Role in Shaping the Global Environment, Geophys. Monogr., No. 85, Amer. Geophys. Union 187-197.

Hibler III, W.D. 1979: A dynamic thermodynamic sea ice model. - Journal of Physical Oceanography 9, 815-846.

Leppäranta, M., Yan, S. & Haapala, J. 1998: Comparison of sea ice velocity fields from ERS-1 SAR and a dynamic model. - Journal of Glaciology, 44 (14) (in press).

Lewis, J.E., Leppäranta, M. & Granberg, H.B. 1993: Statistical properties of sea ice surface topography in the Baltic Sea. - Tellus, 45A, 127-142.

Thorndike, A.S., Rothrock, D.A., Maykut, G.A. & Colony, R. 1975: The thickness distribution of sea ice. - J. Geophys. Res., 80, 4501-4513.

ON THE (NON)CONSERVATION OF MASS IN *PE* OCEAN MODELS

Tapani Stipa

Department of Geophysics
P.O. Box 4, FIN-00014 University of Helsinki, Finland

ABSTRACT

Traditionally, oceanic motions are considered as being non-divergent, which means that their volume is conserved. While this is a good approximation for theoretical analysis and laboratory studies, it leads to inconsistencies when applied to problems where thermodynamics is important. In this case, the ocean mass is adjusted, whereas in nature, the oceans conserve their mass and adjust their volume accordingly. Here the problematics are reviewed, and the beginnings of a volume adjustment formulation presented.

1. INTRODUCTION

The volume of the oceans is determined by the amount of constituents (salts, freshwater) in them and their temperature via the equation of state. Over geological time scales these have varied, so that the volume of the oceans has by no means been constant.

Most numerical models, however, cause a slight distortion to physics by invoking the non-divergence condition, which makes them conserve volume and adjust their mass according to the thermodynamics. This has been a convenient approximation for many theoretical studies and numerical experiments, but it is becoming troublesome for studies of climate drift and thermohaline circulation.

Freshwater is an essential element of the ocean circulation, and it should be trivial to add to the governing equations. Yet it is hard to find in the literature a way of adding freshwater into the ocean in a mass-conserving way — a freshwater flux is essentially an addition of mass in the form of one chemical constituent into the ocean. Most treatments in fluid mechanics deal only with closed systems that may be diabatic (e.g. Batchelor, 1967).

Another problem arises from the thermal expansion of the oceans, due to climatic warming, as discussed by Greatbatch (1994) and Mellor & Ezer (1995). They argue that this effect can be accounted for with a global adjustment of sea level in volume-conserving models, but the physical distortion remains.

It would thus seem desirable to have a mass-conserving ocean model, at least for studies of climate and freshwater cycles (e.g. the BALTEX experiment). This paper discusses the prerequisites for a variable-volume z-coordinate ocean model — a more novel approach is given by Russell & al. (1995). Atmospheric aspects of mass conservation are discussed by e.g. Savijärvi (1995).

2. FORMULATION

Consider a fixed volume V of fluid (cf. Fig. 1). For ease of argumentation let us assume this is in the surface layer of the ocean. This volume contains a mass m composed of a number of fluid molecules and possibly other atoms, i.e. it has a density $\rho = m/V$. At this point it is not necessary to invoke any knowledge of the equation of state for the fluid. We are at liberty to choose the boundaries of this box, so we can choose the upper boundary at $z=\eta$ to lie just outside the fluid, so that $\rho(\eta)=0$ and $\rho(\eta-\varepsilon) > 0$ for any small positive ε.

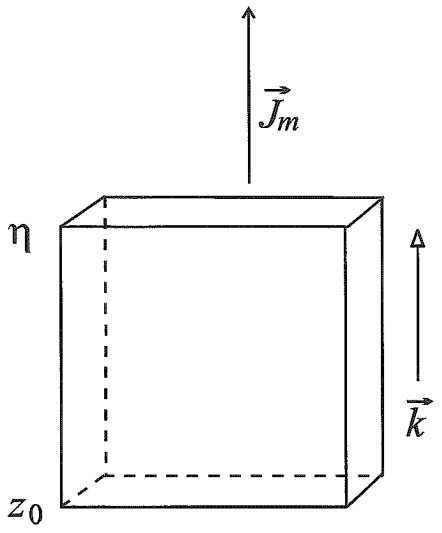

Fig. 1. A sketch of the control volume. η is the upper surface, z_0 the lower surface and $\vec{k}$ the vertical unit vector. The mass flux $\vec{J}_m$ is positive in the positive coordinate direction.

An integral form for the conservation of mass in such a volume can be written as

$$\frac{\partial}{\partial t}\int_V \rho dV + \oint_A \rho\vec{u}\cdot\, d\vec{a} = 0. \tag{1}$$

The vertical extent of the volume in question can vary in time as long as $\partial\eta/\partial t\rho(\eta) = 0$, which is true for our choice of the upper boundary.

The density in this box is a sum of all the constituents, and the velocity should be understood as their mean velocity,

$$\rho = \sum \rho_i + \rho_w \tag{2}$$

$$\vec{u} = \rho^{-1}\left(\sum \rho_i\vec{u}_i + \rho_w\vec{u}_w\right), \tag{3}$$

cf. Fofonoff (1985). The subscript w denotes freshwater and the is are typically salts.

When atoms of any kind (e.g. freshwater) are added to this volume, the mass of the volume will increase, i.e. the density will increase even in the absence of an advective flux. This means that the right hand side of Equation (1) cannot be zero.

Since mass is globally conserved (neglecting conversion to energy) and cannot appear from nowhere, it is most consistent to express the non-zero rhs of Equation (1) as the divergence of a mass flux $\oint_A \vec{J}_m\cdot d\vec{a}$, which after application of the Gauss theorem results in

$$\frac{\partial\rho}{\partial t} + \nabla\cdot(\rho\vec{u}) = \frac{D\rho}{Dt} + \rho\nabla\cdot\vec{u} = -\nabla\cdot\vec{J}_m. \tag{4}$$

This means that a divergent non-advective mass flux going through the control volume will decrease the number of atoms in the control volume. I would like to urge my readers to suppress their intuition of an incompressible fluid for the moment, for this will require information of the equation of state that is not needed at this stage.

The non-zero rhs of Equation (4) has very far-reaching consequences for the conservation properties of all mass-dependent, i.e. extensive quantities. To see this, let us consider the conservation equation for a tracer, say salinity[1] s, that is independent of mass conservation. The most general form for such an equation is the flux form (Haynes & McIntyre, 1990)

$$\frac{\partial(\rho s)}{\partial t} + \nabla\cdot\left(\rho s\vec{u} + \vec{J}_{ds}\right) = 0, \tag{5}$$

i.e. the salt is globally conserved (there is no exchange with the environment, as there is for mass), and it is redistributed by the diffusive flux $\vec{J}_{ds}$ which results from the differential mean motion of salt ions compared to the total mean. For molecular motions, $\vec{J}_{ds}$ is a function of the gradients of chemical potential, heat and pressure (Fofonoff, 1985, Kuiken, 1995), but for macroscopic motions one would opt for an eddy closure.

The diffusion term in Equation (5) is consistent with no mass diffusion in Equation (4) if the definitions of Equations (2) and (3) are adopted for ρ and $\vec{u}$.

Expanding the divergence and the time derivative of Equation (5), one arrives at

$$\rho\frac{\partial s}{\partial t} + s\left(\frac{\partial \rho}{\partial t} + \nabla\cdot(\rho\vec{u})\right) + \rho\vec{u}\cdot\nabla s = -\nabla\cdot\vec{J}_{ds}, \tag{6}$$

which, upon rearrangement and use of Equation (4), results in an equation for the material tendency of s

$$\rho\frac{Ds}{Dt} = -\nabla\cdot\vec{J}_{ds} + s\nabla\cdot\vec{J}_{m}. \tag{7}$$

It is easy to note from Equation (7) that the appearance of the mass flux divergence in the material tendency of salinity is a straightforward consequence of the inclusion of a non-zero rhs in the mass conservation equation (Eq. (4)). This material tendency represents the dilution of salinity by the addition of mass. The term $s\nabla\cdot\vec{J}_m$ can be seen to be equal to the traditional boundary condition for salinity, $s\rho_i(E-P)\delta(\eta-\varepsilon)$ if $\vec{J}_m = \rho_i(E-P)H(\eta-\varepsilon)\vec{k}$ where $H(z)$ is the Heaviside step function, $\delta(z)$ Dirac's δ and E-P is evaporation minus precipitation.

There are two things to note:

1. no "virtual salt flux" need be invoked. Salt is globally conserved and stays within the domain in consideration, and the freshwater enters naturally in the material tendency of salinity as a result of Equation (4), but not in the flux form.
2. the freshwater flux is not a boundary condition for the diffusion of salinity. The appropriate boundary condition is no diffusion through the upper surface, $\vec{J}_{ds}(\eta)\cdot\vec{k} = 0$.

For the sake of consistency, the external mass flux must be taken into account in other conservation equations as well.

The momentum conservation in the flux form reads (Batchelor, 1967)

$$\frac{\partial(\rho\vec{u})}{\partial t} + \nabla\cdot\left(\rho\vec{u}\vec{u} + \vec{p} + \vec{J}_{dm}\right) = -2\vec{\Omega}\times(\rho\vec{u}) - \nabla(\rho\Psi) \tag{8}$$

---

[1] the conserved quantity is the mass of salt ions, ρs. Hence we consider all the components of salinity as one solute, fc. Fofonoff (1985)

which after expansion converts to the familiar equation for the material tendency of velocity

$$\rho\frac{D\vec{u}}{Dt}+\vec{u}\nabla\cdot\vec{J}_m=-\nabla p-2\rho\vec{\Omega}\times\vec{u}-\rho\vec{g}-\nabla\cdot\vec{J}_{dm}. \quad (9)$$

Note that no Boussinesq approximation need be invoked at this stage yet. $\vec{J}_{dm}$ is the diffusive momentum flux due to viscosity (deviatoric stress tensor for molecular motions). Note also that $\nabla\cdot\vec{J}_{dm}=-\mu\nabla^2\vec{u}$ is strictly valid only for a non-divergent flow $(\nabla\cdot\vec{u}=0)$.

The term $\vec{u}\nabla\cdot\vec{J}_m$, which appears due to the addition of mass, does not appear in standard fluid dynamics texts and deserves a little discussion. When the mass flux divergence is positive, i.e. mass is removed from the system as in evaporation, this term results in an accelerating motion, as can be seen from a consideration of the balance $\rho\partial u/\partial t=u\nabla\cdot\vec{J}_m$; if $\nabla\cdot\vec{J}_m > 0$ and $u > 0$, then also $\partial u/\partial t > 0$. On the other hand, if $\nabla\cdot\vec{J}_m > 0$ and $u < 0$, then $\partial u/\partial t < 0$. Conversely, an addition of mass (e.g. precipitation) will cause a deceleration. This result is easily understood when conservation of momentum ρu is considered; if ρ increases, u must decrease and v.v.

This effect is, however, to some extent compensated by the momentum that is transported by J_m, at least in the case of evaporation, so there might be an asymmetry between precipitation and evaporation. The details are probably very involved and outside the scope of this study.

An equation can be written for internal energy per unit volume ρq, but here an external radiative heat flux is taken into account ($\vec{J}_q$). The heat transported by the external mass flux has also to be accounted for; it turns out to be convenient to divide the mass flux into its liquid and vapour components, ($q_m\vec{J}_m=q_{ml}\vec{J}_{ml}+q_{mv}\vec{J}_{mv}$). The internal energy is redistributed by the diffusive flux $\vec{J}_{dq}$:

$$\frac{\partial(\rho q)}{\partial t}+\nabla\cdot(\rho q\vec{u})=-\nabla\cdot(q_m\vec{J}_m)-\nabla\cdot\vec{J}_q-\nabla\cdot\vec{J}_{dq}, \quad (10)$$

where a term $p\nabla\cdot\vec{u}$ has been omitted following common practice. Expanding the derivatives and recognizing that $q_{mv} - q \approx L_v$, L_v being the heat of vaporization, one arrives at

$$\rho\frac{Dq}{Dt}=-L_v\nabla\cdot\vec{J}_{mv}-\nabla\cdot\vec{J}_q-\nabla\cdot\vec{J}_{dq}. \quad (11)$$

3. A VARIABLE VOLUME

Equations (7) and (11) by themselves pose no constraint on the density. The equation of state for seawater, $\rho = \rho\ (T,s,p)$ (Fofonoff, 1985), limits the number of molecules that can be present in a unit volume for certain values of temperature, salinity and pressure. Keeping the pressure constant, a first-order approximation for the material tendency of density can be written as

$$\frac{D\rho}{Dt}=\frac{\partial\rho}{\partial T}\frac{\partial T}{\partial q}\frac{Dq}{Dt}+\frac{\partial\rho}{\partial s}\frac{Ds}{Dt}=-\frac{\alpha\rho}{Cp}\frac{Dq}{Dt}+\beta\rho\frac{Ds}{Dt}, \quad (12)$$

where the common definitions of $\alpha=-\rho^{-1}\frac{\partial\rho}{\partial T}$ and $\beta=\rho^{-1}\frac{\partial\rho}{\partial s}$ have been adopted. These are not constants, but a notational convenience. $C_p \equiv \partial q/\partial T$ is by definition the specific heat at constant pressure and salinity. For simplicity, it is assumed that the thermodynamic processes are reversible.

Using Equations (7) and (11), Equation (12) can be written in terms of the fluxes as

$$\frac{D\rho}{Dt} = \frac{\alpha}{C_p}\left(L_v \nabla\cdot\vec{J}_{mv} + \nabla\cdot\vec{J}_q + \nabla\cdot\vec{J}_{dq}\right) + \beta\left(s\nabla\cdot\vec{J}_m - \nabla\cdot\vec{J}_{ds}\right). \tag{13}$$

If Equation (13) is applied to the mass conservation (Eq. (4)) and integrated in the vertical from z_0 to η, a prognostic equation for $\partial\eta/\partial t = w(\eta)$ is obtained:

$$w(\eta) = \frac{\partial\eta}{\partial t} = -\rho_0^{-1} J_m(\eta) - \frac{\beta}{\rho_0}\left[sJ_m(\eta) - J_{ds}(z_0) + \int_{z0}^{\eta}\nabla_H\cdot\vec{J}_{ds}dz\right] - \int_{z0}^{\eta}\nabla_H\cdot\vec{u}dz + w(z_0)$$
$$-\frac{\alpha}{\rho_0 C_p}\left[J_q(\eta) - J_q(z_0) + L_v J_{mv}(\eta) + J_{dq}(\eta) - J_{dq}(z_0) + \int_{z0}^{\eta}\nabla_H\cdot\vec{J}_{dq}\mathrm{d}z\right]. \tag{14}$$

The free surface development thus has a direct contribution from the mass flux, thermodynamic contributions from the heat and mass fluxes, and horizontal velocity divergence as well as the vertical velocity at the bottom boundary of integration.

Equation (14) compares directly to a similar equation by Greatbatch (1994, Eq. (5)) with the exception that it is derived in a more general, consistent way. There is no need to invoke a kinematic boundary condition for volume as done by Huang (1993) to include the effect of freshwater — in fact, this is inconsistent with the mass conservation as adapted by Greatbatch (1994), since the real direct effect of precipitation on the velocity divergence is $\frac{\rho_i}{\rho_0}P$. The difference, about 2-3 %, is admittedly small but systematic, and therefore a potential source of problems.

4. DISCUSSION AND CONCLUSIONS

I have presented a consistent way of deriving the conservation equations of oceanic motions in the presence of an external mass flux. Such a formulation is necessary in order to properly account for the effect of the addition of freshwater into the ocean.

As a result, it is possible to derive a prognostic equation for the sea surface elevation that takes the steric effect into account and can therefore be used for e.g. altimetry studies and in coastal areas where this effect is significant, and possibly even in long-term integrations without an arbitrary correction. An obvious conclusion is that a numerical model that allows for thermodynamics should also allow for a change in the volume of oceans by a corresponding amount.

However, there are numerical problems caused by a divergent flow field. Many z-coordinate models do explicitly exploit the non-divergence condition, and would therefore need considerable redesign to cope with divergence. A domain varying in both space and time also results in discretization problems, conceptually comparable to a time-varying bottom topography. There is thus still some room for development in the way we model the oceans.

Acknowledgements

I am grateful for comments from Gavin Schmidt, George Russell and Markus Meier in the early stages. An intense late night discussion with Martin Schmidt help me sharpen the argumentation, and convinced me that this idea was worth writing down. I also thank the Maj and Tor Nessling foundation for tolerating my side roads during the years and for making this work financially possible.

REFERENCES

Batchelor, G.K. 1967: An introduction to Fluid Dynamics. - Cambridge University Press.

Fofonoff, N.P. 1985: Physical properties of seawater: A new salinity scale and equation of state for seawater. - Journal of Geophysical Research, 90:3332-3342.

Greatbatch, R.J. 1994: A note on the representation of steric sea level in models that conserve volume rather than mass. - Journal of Geophysical Research, 99:12767-12771.

Haynes, P.H. & McIntyre, M.E. 1990: On the conservation and impermeability theorems for potential vorticity. - Journal of the Atmospheric Sciences, 47:2021-2031.

Hill, N.M. (ed), 1962: The Sea. Vol. 1. - Interscience publishers.

Huang, R.X. 1993: Real freshwater flux as a natural boundary condition for the salinity balance and thermohaline circulation forced by evaporation and precipitation. - Journal of Physical Oceanography, 23:2428-2446.

Kuiken, G.D. 1995: Thermodynamics of Irreversible Processes. - Wiley.

Mellor, G.L. & Ezer, T. 1995: Sea level variations induced by heating and cooling: An evaluation of the Boussinesq approximation in ocean models. - Journal of Geophysical Research, 100:20565-20577.

Russell, G.L., Miller, J.R. & Rind, D. 1995: A coupled atmosphere-ocean model for transient climate change studies. - Atmosphere-Ocean, 33:683-730.

Savijärvi, H. 1995: Water mass forcing. - Beitr. Phys. Atmosph., 68:75-84.

MEASURED AND MODELLED LATENT HEAT FLUX OVER THE BALTIC SEA

Anna Rutgersson

Swedish Meteorological and Hydrological Institution, Uppsala University
SE-601 76 Norrköping, Sweden

ABSTRACT

Direct measurements of latent heat flux over the Baltic Sea are compared with the latent heat flux calculated with two different models. The atmospheric model (HIRLAM) is a 3D regional scale numerical weather prediction model and the ocean model (PROBE-Baltic) is a 10 basin model. Both HIRLAM and PROBE-Baltic overestimate the latent heat flux for the investigated period. Some tests with HIRLAM are also performed, and it is shown that changing the surface parameterization will improve the latent heat flux. Such improvements will not necessarily lead to an improvement in other parameters such as the two-metre values of temperature and humidity.

1. INTRODUCTION

Surface fluxes of momentum, sensible and latent heat are of great importance for climate simulations and longer forecasts, but will also influence the near-surface parameters for shorter forecasts. To get correct fluxes and thus correct forecasts it is of importance to have the correct surface values of temperature and humidity and also to describe the physics of transfer in a proper way. Since there exist very few direct flux measurements, especially over the sea, there are still things to investigate in that area. In Rutgersson (1998), the surface flux of momentum and sensible heat in HIRLAM have been shown to agree rather well with measured fluxes for an extended time period. In an earlier study it was indicated that HIRLAM gives too large a latent heat flux (Gustafsson & al., 1998). Here the HIRLAM meteorological model and the PROBE-Baltic oceanographic model are used, and the resulting fluxes are compared with direct measurements. Different versions of the surface flux parameterization in HIRLAM are tested.

2. THEORY

The surface turbulent fluxes are determined from mean model parameters using the bulk formulation. The transfer coefficients for momentum (C_D), sensible (C_H) and latent heat (C_E) are described by:

$$C_D = \kappa^2 \left(ln \frac{z}{z_0} \right)^{-2}$$

$$C_H = C_D^{1/2} \kappa \left(ln \frac{z}{z_{0T}} \right)^{-1} \qquad (1)$$

$$C_E = C_D^{1/2} \kappa \left(ln \frac{z}{z_{0q}} \right)^{-1}$$

where κ is the von Kármán constant, z the measuring height and z_0, z_{0T} and z_{0q} are the roughness lengths for momentum, sensible and latent heat, respectively. The sea roughness can be described by the Charnock's formula, $z_0 = \alpha \cdot u_*^2 / g$, where α is a constant. This gives a strong, nearly linear

wind speed dependence which is well established by several studies Smith, 1980, Donelan, 1990, Maat & al., 1991). The value of α varies in the literature between 0.011 (Smith, 1980) up to over 0.03 (Smith & al., 1992). In HIRLAM a high value (0.032) is used, and the roughness lengths for heat and humidity (z_{0T} and z_{0q}) are taken as equal to the stress roughness length (z_0). This gives a strong wind speed dependence in the heat fluxes also, something which can *not* be supported by measurements (Smith, 1989, DeCosmo & al., 1996). In this study three different ideas for new formulations in HIRLAM are studied and compared for an extended period.

2.1 Case 1 (constant coefficients)

Sensible and latent heat flux exchange coefficients are often taken as constants, apart from their stability dependence. Common values are those from the HEXOS experiment, (DeCosmo & al., 1996) $C_{H10} = C_{E10} = 1.1 \cdot 10^{-3}$. In HIRLAM the fluxes are calculated as a difference between the surface and the lowest model level (~ 30 m), so a lower value than the HEXOS results was used for this test, $C_H = C_E = 0.9 \cdot 10^{-3}$ f(Ri, z/z_0). Ri is the bulk Richardson number.

2.2 Case 2 (the Makin case)

A slight wind speed dependence is not ruled out by the rather scattered measurements. If z_{0T} is independent of wind speed it follows that $C_H \sim C_D^{1/2}$. This is described more carefully in Makin (1998). The formulation $C_H = C_E = \beta C_{DN}^{1/2} f(Ri, z/z_0)$ where $\beta = 2.9 \cdot 10^{-2}$ was tested in HIRLAM. The stability dependence is the same as in the reference version. This formulation has also been tested by Makin & Perov (1997) for a shorter period, with very promising results.

2.3 Case 3 (the Beljaars case)

This case is based on the formulation used in the ECMWF model and is described in detail in Beljaars (1995). The equations for the stability dependence are solved explicitly by iterations, and different roughness lengths are used for heat ($z_{0T} = 0.40\nu/u_*$), humidity ($z_{0q} = 0.62\nu/u_*$) and momentum ($z_0 = 0.11\nu/u_* + 0.018 \cdot u_*^2/g$), ν is the kinematic viscosity of air. This gives transfer coefficients which are large for very light winds, representing a situation with a smooth surface or gustiness at low wind speeds, decreasing to a minimum at ~ 4 m/s and slightly increasing for higher wind speeds.

3. MODELS AND MEASUREMENTS

For the HIRLAM tests version 4.2.2 has been used with non-local turbulent diffusion, a horizontal resolution of 55 km and 31 levels in the vertical. The ocean model PROBE-Baltic (Omstedt & Nyberg, 1996) is a basin model which also includes ice. The measurements have been made at a small island east of Gotland (Östergarnsholm) on a site that nearly represents marine conditions. The measurements are explained in detail in Smedman & al. (1999) and Rutgersson (1998).

4. RESULTS

From February 7 to February 22, 1997, 6-hour forecasts have been run at every 6th hour for the different cases. Figure 1a) shows the latent heat flux from the HIRLAM reference run and Case 2 together with the PROBE-Baltic simulation. In Figure 1b) the difference between the reference case and the test cases are shown. All cases using HIRLAM and PROBE-Baltic overestimate the modelled latent heat flux compared to the measured fluxes, especially during the period with high wind speed, February 18. The three test cases give in general smaller fluxes than the reference run. Differences vary from -10 W/m^2 up to 50 W/m^2, depending on the situation. The difference between

the cases is largest during the high wind speed situations. The temperature and humidity in the test cases differ very little from each other and are all warmer and more humid than the reference case.

RMS and BIAS for the HIRLAM cases are calculated using 12 coastal synoptic stations in Sweden and Finland. The results are shown in Figure 2. Errors in 2 metre temperatures show similar results as those for the dew point, but with smaller magnitudes. The error in the 2 metre dew point is larger for all test cases than that for the reference run. This is especially so around February 15 when there is a cold air outbreak with large fluxes. Only for Case 3 around the 17th is there a slight improvement. For other parameters, the differences are small. Case 3 shows a slight improvement for wind speed and sea level pressure, possibly explained by the revised formulation of z_0.

The vertical profiles of temperature and humidity are verified against several radiosondes for February 8, Figure 3. There is a certain improvement in the vertical distribution of humidity for this situation. Case 1 shows the best behaviour at 600-800 hPa but the other test cases also show a better result than the reference case.

5. CONCLUSIONS

These results are somewhat contradictory. What appears to be an improvement in all the HIRLAM test cases with decreased surface fluxes is accompanied by large RMS errors and BIAS in temperature and dew point. The more physical schemes did give an improvement in fluxes, but not in mean parameters. Too high transfer coefficients in the old formulation could compensate for some other deficiency in the model. Similar results were seen in Beljaars (1994), where the more physically correct scheme did not improve the surface parameters in general. Beljaars suggested this could be explained by errors in the convection scheme. If the convection scheme is not efficient enough to dry out the model properly, the lowest levels will be too humid. This hypothesis is supported by the fact that the largest errors are seen during the cold air outbreak on February 15. The increase in the transfer coefficients in the low winds in Case 3 in the smooth surface regime did improve the dew point on February 17, when there were low winds. The vertical distribution of dew point is improved, which could also be seen in Makin & Perov (1997) with the revised scheme. Decreased surface fluxes give a cooling of the lower part of the boundary layer. Perhaps longer simulations than 6 hours might show some effect on clouds and precipitation, but that cannot be seen in this study. The final conclusions are:

- The different test cases using HIRLAM do not differ very much from each other, but they differ from the reference simulation.
- A new formulation of surface fluxes in HIRLAM would improve the latent heat fluxes over the sea.
- The larger errors in 2 metre temperature and humidity need to be considered, and perhaps a completely new formulation needs to be developed.
- The PROBE-Baltic ocean model also overestimates the latent heat fluxes for the studied period; this can probably to a large extent be explained by the surface flux parameterization scheme.

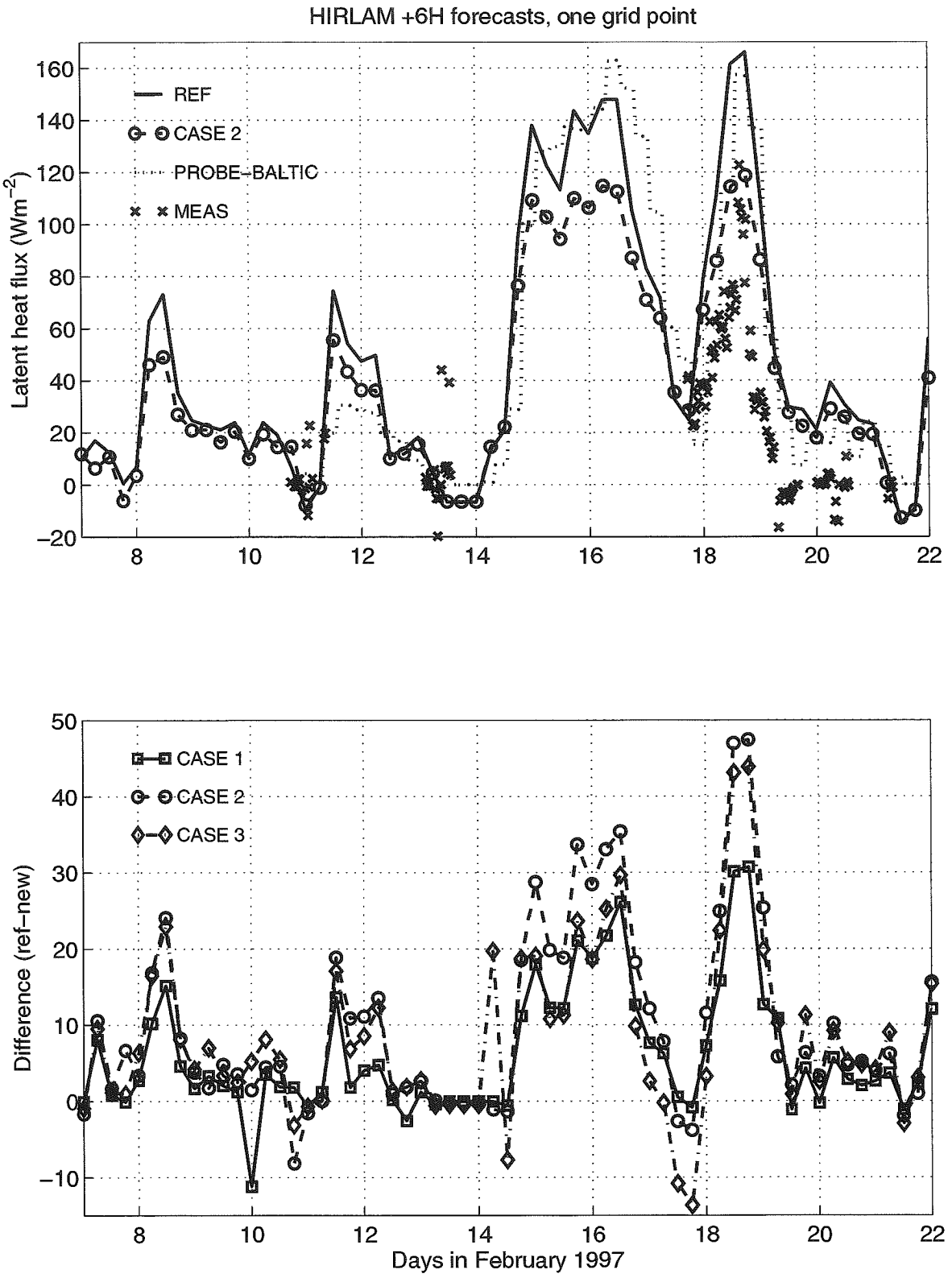

Fig. 1. a) Latent heat flux from one grid point within the Baltic Sea using HIRLAM; each value represents a 6 hour forecast, the solid line is reference version 4.2.2, circles represent Case 2. The dotted line is PROBE-Baltic and crosses are direct measurements. b) Difference in latent heat between reference HIRLAM and the different cases. Squares are reference case minus Case 1, circles reference minus Case 2 and diamonds reference minus Case 3.

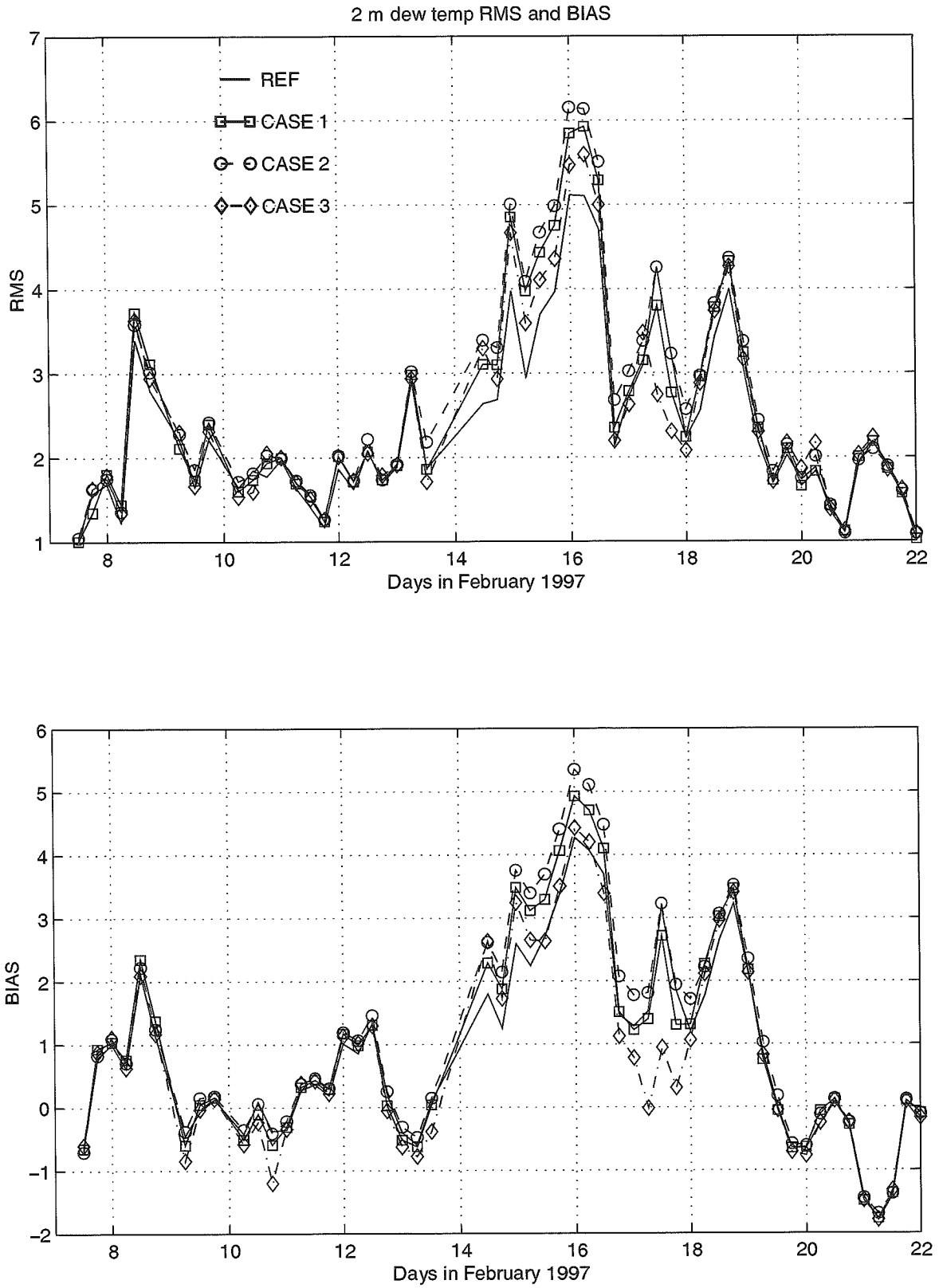

Fig. 2. RMS and BIAS for the 2 metre dew point in HIRLAM. 12 coastal synoptic stations are used for the error calculations. The solid line is the reference version, squares are Case 1, circles Case 2 and diamonds Case 3.

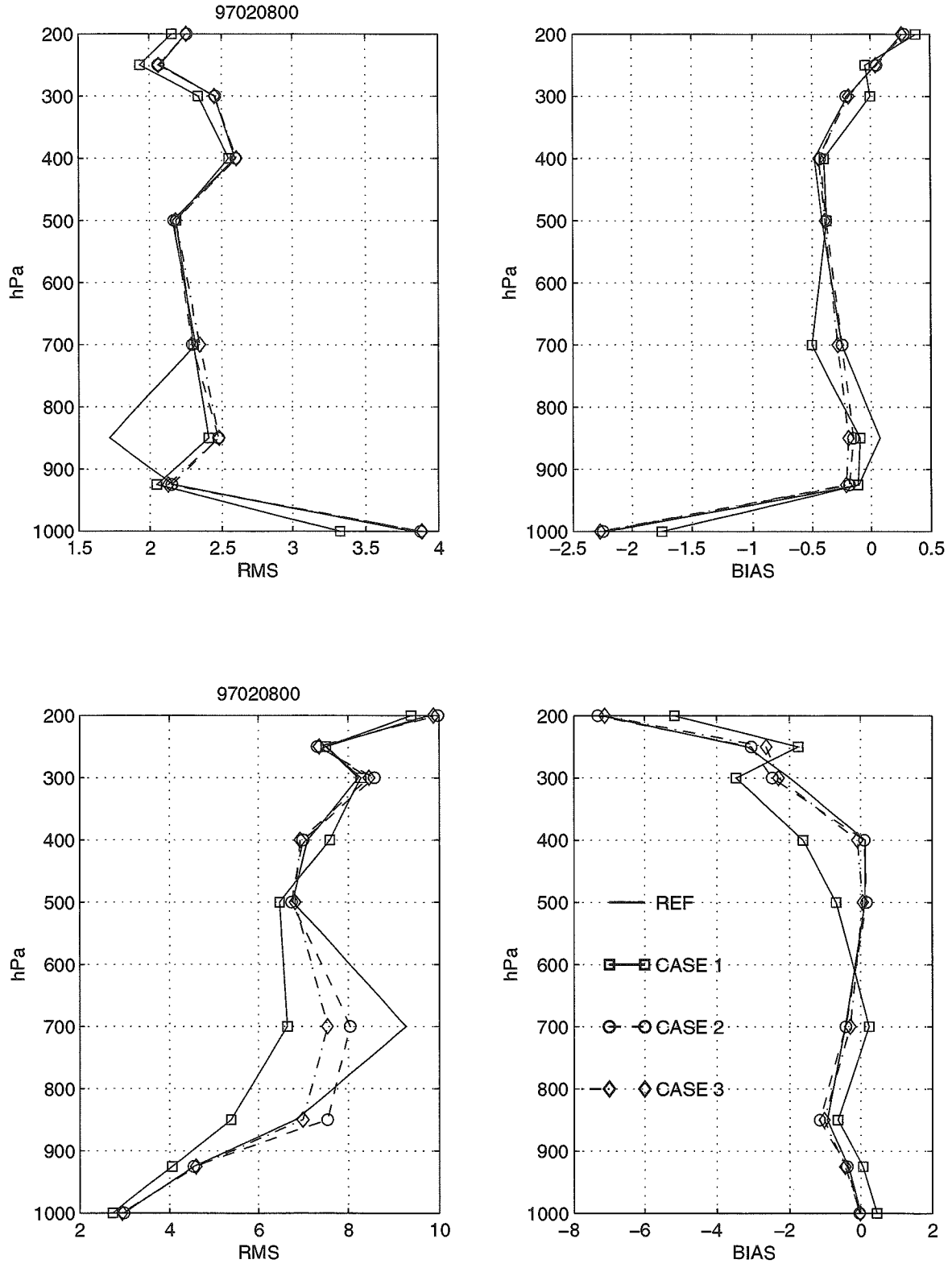

Fig. 3. a) Vertical profiles of RMS error for the temperature in HIRLAM. The solid line is the reference version, squares are Case 1, circles Case 2 and diamonds Case 3. b) Vertical profiles of BIAS for the temperature. c) Vertical profiles of RMS error for the dew point. d) Vertical profiles of BIAS for the dew point.

REFERENCES

Beljaars, A.C.M. 1994: The parametrization of surface fluxes in large scale models under free convection. - Quart. J. Roy. Meteor. Soc., 212:255-270.

Beljaars, A.C.M. 1995: The impact of some aspects of the boundary layer scheme in the ECMWF model. - In: Parameterization of sub-grid scale physical processes, pp. 125-161.

DeCosmo, J., Katsaros, K.B., Smith, S.D., Anderson, R.J., Oost, W.A., Bumke, K. & Chadwick, H. 1996: Air-sea exchange of water vapour and sensible heat: The HEXOS results. - J. Geophys. Res. 101:12001-12016.

Donelan, M.A. 1990: Air-sea interaction. - In: LeMehaute, B. & Hanes, D. (eds.), The Sea: Ocean Engineering Science, Vol. 9, pp 239-292, John Wiley, New York.

Gustafsson, N., Nyberg, L. & Omstedt, A. 1998: Coupling High Resolution Atmosphere and Ocean Models for the Baltic Sea. - Mon. Wea. Rev., 126:2822-2846.

Maat, N., Kraan, C. & Oost, A. 1991: The roughness of wind waves. - Bound.-Layer Meteor., 54:89-103.

Makin, V.K. 1998: A note on wind speed and sea state dependence of the heat exchange coefficient. - Submitted to Bound.-Layer Meteor.

Makin, V.K. & Perov, V. 1997: On the Wind Speed Dependence of Momentum, Sensible Heat and Moisture Exchange Coefficients Over Sea in the HIRLAM Model - a case study. - Hirlam Newsletter, 29:26-31.

Omstedt, A. & Nyberg, L. 1996: Response of Baltic Sea ice to seasonal, interannual forcing and climate change. - Tellus, 48A:644-662.

Rutgersson, A. 1998: A comparison between measured and modeled sensible heat and momentum fluxes using a High Resolution Limited Area Model (HIRLAM). - Submitted to Contr. Atm. Phys.

Smedman, A.-S., Högström, U., Bergström, H., Rutgersson, A., Kahma, K.K. & Pettersson, H. 1999: A case-study of air-sea interaction during swell conditions. - Accepted to J. Geophys. Res.

Smith, S.D. 1980: Wind stress and heat flux over the ocean in gale force winds. - J. Geophys. Res., 10:709-726.

Smith, S.D. 1989: Water vapour flux at the sea surface. - Bound.-Layer Meteor., 47:277-293.

Smith, S.D., Anderson, R.J., Oost, W.A., Kraan, C., Maat, N., DeCosmo, J., Katsaros, K.B., Davidson, K.L., Bumke, K., Hasse, L. & Chadwick, H.M. 1992: Sea surface wind stress and drag coefficients: The HEXOS results. - Bound.-Layer Meteor., 60:109-142.

COUPLING WAVES WITH THE ATMOSPHERE - CONSEQUENCES FOR THE HEAT EXCHANGE COEFFICIENT

V.K. Makin

Royal Netherlands Meteorological Institute (KNMI)
P.O. Box 201, 3730 AE De Bilt, The Netherlands

ABSTRACT

The wind over waves coupling theory, which allows us to relate the drag coefficient to the properties of the sea surface and the properties of the momentum exchange at the sea surface, is discussed shortly. The resistance law above the sea is derived, and the explicit relation for the heat exchange coefficient C_H is obtained. It is shown that C_H follows a square-root dependence on the drag coefficient C_D. However, the proportionality coefficient appears to depend on the sea state, expressed in terms of the coupling parameter. Dependence on the sea state suppresses the $C_D^{1/2}$ wind speed dependence, and results in a marginal increase of C_H with increase in wind speed.

1. INTRODUCTION

Momentum and heat fluxes above the sea depend in general both on the wind speed and the sea state (Janssen, 1989; Chalikov & Makin, 1991; Makin & al., 1995; Makin & Mastenbroek, 1996; Makin, 1998; Makin, 1999; Makin & Kudryavtsev, 1999). The wind over waves coupling theory relates the sea drag coefficient to the properties of the sea surface and the momentum exchange at the sea surface. The approach is based on the conservation of momentum in the marine surface atmospheric boundary layer, which implies that the total stress is independent of height, so that the momentum flux at a given height is equal to the momentum flux at the sea surface.

The total stress is supported by turbulent motions of the air and by organised wave-induced motions due to the presence of waves. The former can be calculated using a local eddy-viscosity closure, the latter is related to the directional spectrum of sea waves and the wave growth rate parameter.

Wave-induced stress plays an important role in the exchange of momentum at the sea surface. While at low wind speeds it supports only a marginal part of the total stress at the surface, it becomes dominant in moderate to strong winds. The fact that the wave-induced stress increases with wind speed leads to a strong wind speed dependence of the drag coefficient. The drag coefficient increases approximately linearly with increase in wind speed.

It has been well established by field measurements that the heat (sensible and latent) exchange coefficient over the sea is much less dependent on wind speed than the drag coefficient (Anderson, 1993; DeCosmo & al., 1996; Friehe & Schmitt, 1976; Geernaert, 1990; Large & Pond, 1982; Smith, 1980, 1988, 1989). However, the actual wind-speed dependence of the heat exchange coefficient is obscured, because difficulties in heat-flux measurements result in a considerable scatter of data. The heat exchange coefficient C_H is usually parameterized as a constant, i.e. the wind speed independent $C_H = Const.$ (Anderson, 1993; DeCosmo & al., 1996; Friehe & Schmitt, 1976; Large & Pond, 1982; Smith, 1980, 1988, 1989), with the constant having a value of about 10^{-3}.

However, a dependence on wind speed is not ruled out by the field measurements. Large & Pond (1982) argue that for wind speeds above 10 m s^{-1} the parameterization of the heat exchange coefficient in terms of a constant temperature roughness length is more appropriate, though the statistical improvement of such a fit to their data is not significant compared to the constant heat exchange coefficient parameterization. Assuming the logarithmic distribution of temperature, it immediately follows that in this case

$$C_H = c_1 C_D^{1/2} \tag{1}$$

where C_D is the momentum exchange coefficient (the drag coefficient), and c_1 is a constant. For high wind speeds, the dependence (1) overestimates the heat exchange coefficient, compared to the constant value of C_H, by more than 50 %.

The different wind-speed dependence of the drag coefficient and the heat exchange coefficient can be explained by the difference in exchange mechanisms of momentum and heat close to the sea surface (Makin & Mastenbroek, 1996). Momentum is transported to a large extent by the organised wave-induced motions correlated with the waves (the wave-induced stress). With increase in wind speed the wave-induced stress increases, which results in the growth of the drag coefficient (Makin & al., 1995). The wave-induced flux of heat plays a negligible role in the heat transport (Makin & Mastenbroek, 1996), so that waves cannot directly influence the exchange of heat over the sea. The heat transport is fully determined by the turbulence above the waves, and by the molecular processes in the laminar sub-layer next to the surface.

Assuming a local balance between the production of turbulent kinetic energy (the TKE production) and its dissipation, an explicit relation for the heat exchange coefficient can be obtained. The heat exchange coefficient follows a $C_D^{1/2}$ dependence; however, the proportionality coefficient is not a constant but depends on the sea state, described in terms of the coupling parameter α (the ratio of the wave-induced stress at the surface to the total stress). This dependence on α suppresses the $C_D^{1/2}$ increase of C_H, resulting in only a slight increase of C_H with increase in wind speed.

2. RESISTANCE LAW ABOVE WAVES

Above waves the total stress is supported by the mean turbulent stress $\tau^t = -\overline{u'w'}$ and the wave-induced stress τ^w due to the organized wave motions in the atmosphere induced by the waves (Janssen, 1989; Chalikov & Makin, 1991; Makin & al., 1995; Makin & Kudryavtsev, 1999)

$$\tau^t(z)+\tau^w(z)=u_*^2, \tag{2}$$

and by definition equals the square of the friction velocity u_*.

The local turbulence closure relates the turbulent flux to the gradient of the velocity field u via the eddy viscosity K

$$\tau^t(z)=K\frac{\partial u}{\partial z}. \tag{3}$$

From (2) and (3)

$$K\frac{\partial u}{\partial z}=u_*^2-\tau^w(z). \tag{4}$$

If the sea surface is assumed to be a superposition of random waves of all scales, characterized by a directional wave spectrum $S(k, \phi)$ (k is the wave number which satisfies the gravity-capillary dispersion relation, ϕ is the propagation direction of the k-wave component relative to the wind direction), the wave-induced stress can be written

$$\tau^w(z)=\tau^w(0)f(z) \tag{5}$$

Here $\tau^w(0)$ is the form drag

$$\tau^w(0)=\int_0^\infty \tau(k)d(\ln k), \tag{6}$$

τ is the omnidirectional spectrum of the momentum flux to the waves

$$\tau(k)=\int_{-\pi}^{\pi} c^2\, B(k,\phi)\beta(k,\phi)\cos\phi d\phi \tag{7}$$

$B(k, \phi) = k^4 S(k, \phi)$ is a saturation spectrum, c is the phase velocity, $\beta(k, \phi)$ is the growth rate parameter describing the energy flux to the waves from the atmosphere (see Makin & Kudryavtsev, 1999), and $f(z)$ is a dimensionless function describing the vertical decay of the mean wave-induced stress. The function $f(z)$ is defined as

$$f(z)=\frac{1}{\tau^w(0)}\int_0^\infty \tau(k)F(k,z)d(\ln k) \tag{8}$$

where $F(k,z)$ is another dimensionless function describing the vertical distribution of the individual wave components. The function $F(k,z)$ decays with height and satisfies the condition $F(k, z_0^v)=1$ at the surface, so that the decay function $f(z)$ also equals 1 at the surface and decays rapidly with height above the waves (Makin & Mastenbroek, 1996; Makin & Kudryavtsev, 1999).

In terms of the coupling parameter

$$\alpha=\frac{\tau^w(0)}{u_*^2}, \tag{9}$$

and the decay function of the wave-induced stress, equation (4) is rewritten as

$$K\frac{\partial u}{\partial z}=u_*^2\,(1-\alpha f(z)). \tag{10}$$

The eddy viscosity K above the waves is obtained through the local balance between the TKE production P and its dissipation to heat ε (Chalikov & Belevich, 1993; Makin & Mastenbroek, 1996; Makin & Kudryavtsev, 1999)

$$P = \varepsilon. \tag{11}$$

The production of the TKE P above the waves results from the mean and the wave-induced motions (Makin & Mastenbroek, 1996) and equals

$$P=(\tau^t+\tau^w)\frac{\partial u}{\partial z}=u_*^2\frac{\partial u}{\partial z}. \tag{12}$$

Using the mixing length theory, and expressing the dissipation in terms of K and the mixing length $l = \kappa z$ (κ is the von Kármán constant), $\varepsilon = K^3 l^{-4}$, the equation for the eddy viscosity is found from (10), (11) and (12):

$$K=lu_*(1-\alpha f(z))^{1/4}. \tag{13}$$

The resistance law above the sea in terms of the drag coefficient,

$$C_D=\left(\frac{u_*}{u_{10}}\right)^2, \tag{14}$$

where u_{10} is the wind speed at a height of 10 m, follows immediately from (10) and (11):

$$C_D^{1/2} = \frac{u_*}{u_{10}} = \kappa \left(\int_{z_0^\nu}^{10} [1 - \alpha f(z)]^{3/4} \, d(\ln z) \right)^{-1}. \tag{15}$$

To obtain (15) integration is carried out from the viscous roughness length z_0^ν to a height of 10 m. Makin & al. (1995) have shown that the viscous roughness length is related to the surface turbulent stress $\tau^t(0) = u_*^2(1-\alpha)$ through

$$z_0^\nu = 0.1 \frac{\nu}{u_* (1-\alpha)^{1/2}} \tag{16}$$

where ν is the kinematic viscosity of the air. The coupling parameter in (15) can be expressed via (6)

$$\alpha = \frac{1}{u_*^2} \int_0^\infty \tau(k) d(\ln k). \tag{17}$$

Relation (15) relates the drag of the sea surface directly to the properties of the momentum exchange at the surface via the coupling parameter (17) and the vertical distribution of the wave-induced stress $f(z)$, equation (8). The coupling parameter is determined by the geometrical properties of the surface via the directional wavenumber wave spectrum $S(k, \phi)$, and by the peculiarities of the energy exchange between wind and waves, expressed via the growth rate parameter. The growth rate parameter, as shown by Makin & Kudryavtsev (1999), depends in turn on the drag coefficient (the friction velocity), and the coupling parameter. Equations (15) and (17) are solved by iterations after the form of the wave spectrum $S(k, \phi)$ is given by a functional relation or is specified by a physical model based on the solution of the wave energy balance equation.

3. THE HEAT EXCHANGE COEFFICIENT

Above the waves the heat flux is supported only by turbulence (Makin & Mastenbroek, 1996), whence

$$-\overline{\theta' w'} = K \frac{\partial \theta}{\partial z} = \theta_* u_*, \tag{18}$$

where θ_* is the temperature scale. This flux is constant with height in the atmospheric surface layer. From (18), (13), and (14) the heat exchange coefficient can be obtained as:

$$C_H = \frac{\theta_* u_*}{u_{10} \Delta\theta} = \kappa C_D^{1/2} \left(\int_{z_0^\nu}^{10} [1 - \alpha f(z)]^{-1/4} \, d(\ln z) \right)^{-1}. \tag{19}$$

where above, $\Delta\theta$ is the temperature difference between a height of 10 m and the surface. What follows immediately from (19) is that the heat exchange coefficient is proportional to $C_D^{1/2}$, with the proportionality coefficient dependent upon the coupling parameter α. If the sea state dependence in (19) is ignored, or if it is assumed that the coupling parameter is a slowly-varying function of wind speed, relation (1) is recovered.

However, the coupling parameter is a strongly-varying function of the wind speed. The wind-speed dependence of the coupling parameter is shown in Figure 1. This dependence is obtained by the Makin & Mastenbroek (1996) model. The data of Banner & Peirson (1998), though with only two available experimental points, seem to support the model prediction.

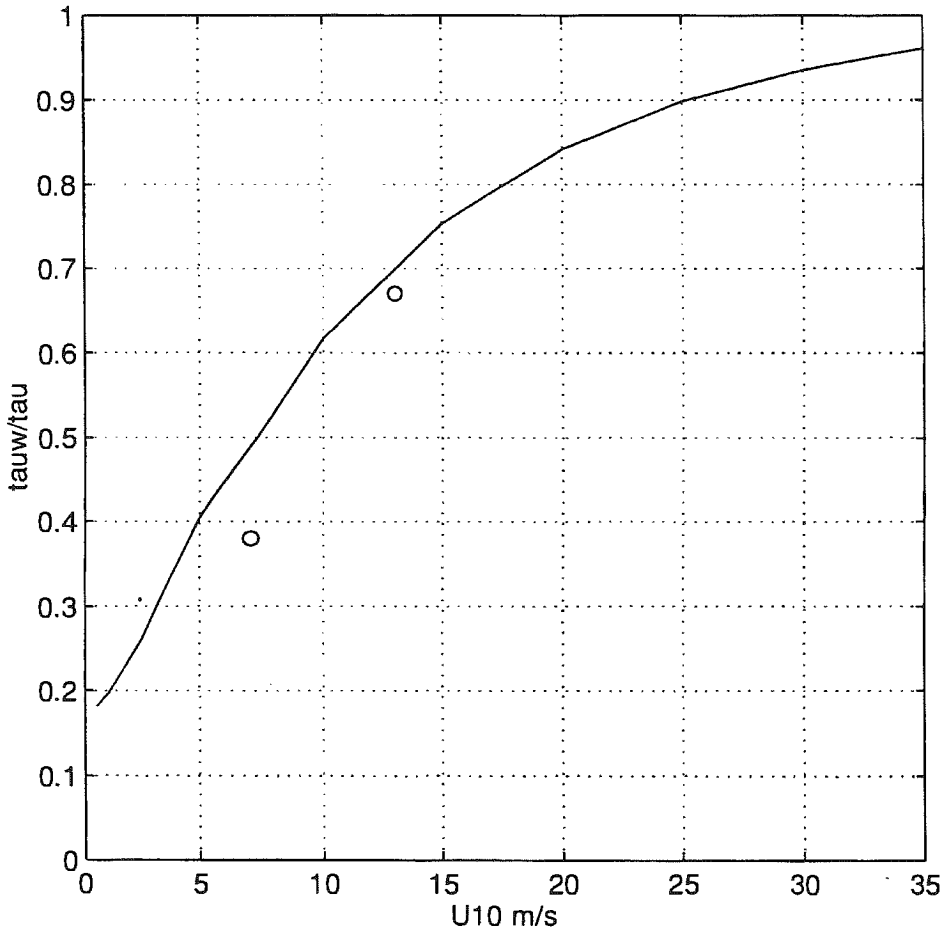

Fig. 1. The coupling parameter α versus u_{10}. Circles - experimental data of Banner & Peirson (1998).

The heat exchange coefficient, calculated according to (19), is shown in Figure 2, together with the open ocean data of Anderson (1993). The dependence of C_H on the coupling parameter suppresses the $C_D^{1/2}$ dependence on the wind speed, resulting in a slower increase of the heat exchange coefficient with wind speed compared to the dependence (1). For high wind speeds the difference in C_H between (1) and (19) can reach 20 % or more.

To obtain a simple parameterization for C_H, the integral in (19) is approximated by $13.2(1-0.75\ \alpha)^{-1/4}$, which gives

$$C_H = 0.031 C_D^{1/2} (1 - 0.75\alpha)^{1/4} \tag{20}$$

Relation (20) reasonably approximates (19) (see Figure 2) and can be used in applied studies.

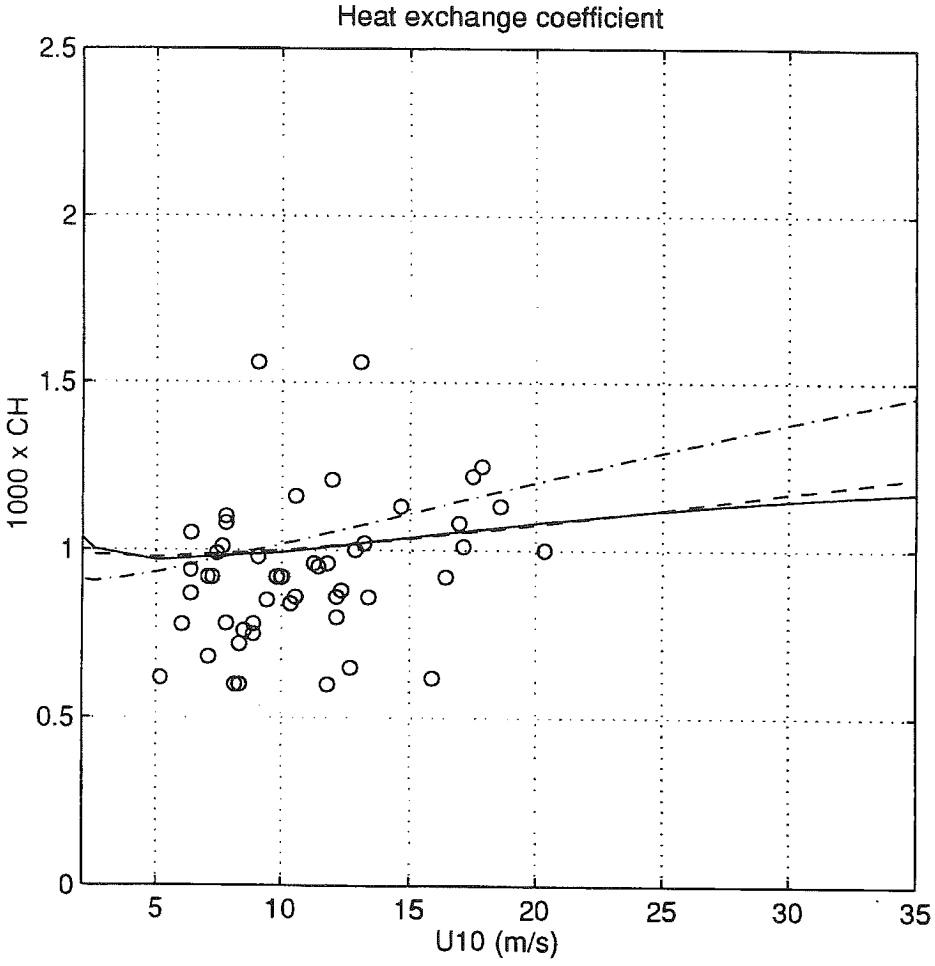

Fig. 2. The heat exchange coefficient C_H versus u_{10}. Solid line - relation (19); dashed line - relation (20); dashed-dotted line - dependence (1) with $c_1 = 0.027$. Circles - experimental data of Anderson (1993).

4. DISCUSSION

The resistance law above the sea has been derived. It is related to the sea state (in terms of the directional wave spectrum) and properties of the momentum exchange at the sea surface. An explicit relation for the heat exchange coefficient C_H is obtained. It is shown that C_H depends on the square root of the drag coefficient C_D. However, the proportionality coefficient appears to depend on the sea state, expressed in terms of the coupling parameter. Dependence on the sea state suppresses the $C_D^{1/2}$ wind-speed dependence, and results in a marginal increase of C_H with increase in wind speed.

Though experimental data do not distinguish between the wind-speed dependence of the heat exchange coefficient (1), (19), or $C_H = Const.$ because of the large scatter in data, it is thought that use of the physically-based relation (19) is preferable in applied studies. It relates C_H not only to the drag coefficient, but to the sea state too.

It is worthwhile mentioning here that sea spray may play a role in heat (sensible and latent) exchanges at the sea surface at wind speeds of about 25 m s^{-1} and above (Makin, 1998). In this case the generalized explicit relations for the sensible heat and humidity exchange coefficients that account for the sea spray effects can easily be obtained by substituting expression (13) for the eddy viscosity coefficient K obtained in the present paper into equations (67)-(72) in Makin (1998).

REFERENCES

Anderson, R.J. 1993: A study of wind stress and heat flux over the open ocean by the inertial-dissipation method. - J. Phys. Oceanogr., 23:2153-2161.

Banner, M.L. & Peirson, W.L. 1998: Tangential stress beneath wind-driven air-water interfaces. - J. Fluid Mech., 364:115-145.

Chalikov, D.V. & Belevich, M.Yu. 1993: One-dimensional theory of the wave boundary layer. - Boundary-Layer Meteorol., 63:65-96.

Chalikov, D.V. & Makin, V.K. 1991: Models of the wave boundary layer. - Boundary-Layer Meteorol., bf 56:83-99.

DeCosmo, J., Katsaros, K.B., Smith, S.D., Anderson, R.J., Oost, W.A., Bumke, K. & Chadwick, H. 1996: Air-sea exchange of water vapor and sensible heat: The Humidity Exchange Over the Sea (HEXOS) results. - J. Geophys. Res., 101:12001-12016.

Friehe, C.A. & Schmitt, K.F. 1976: Parameterizations of air-sea interface fluxes of sensible heat and moisture by the bulk aerodynamic formulas. - J. Phys. Oceanogr., 6:801-809.

Geernaert, G.L. 1990: Bulk parameterizations for the wind stress and heat fluxes. - Surface Waves and Fluxes, Vol. 1, G.L. Geernaert and W.J. Plant, (Eds.), Kluwer Academic, 336 pp.

Janssen, P.A.E.M. 1989: Wave-Induced Stress and the Drag of Air Flow over Sea Waves. - J. Phys. Oceanogr., 19:745-754.

Large, W.G. & Pond, S. 1982: Sensible and latent heat flux measurements over the ocean. - J. Phys. Oceanogr., 12:464-482.

Makin, V.K. 1998: Air-sea exchange of heat in the presence of wind waves and spray. - J. Geophys. Res., 103:1137-1152.

Makin, V.K. 1999: A note on wind speed and sea state dependence of the heat exchange coefficient. - Boundary-Layer Meteorol., in press.

Makin, V.K. & Kudryavtsev, V.N. 1999: Coupled sea surface--atmosphere model 1. Wind over waves coupling. - J. Geophys. Res., in press.

Makin, V.K. & Mastenbroek, C. 1996: Impact of waves on air-sea exchange of sensible heat momentum. - Boundary-Layer Meteorol., 79:279-300.

Makin, V.K., Kudryavtsev, V.N. & Mastenbroek, C. 1995: Drag of the sea surface. - Boundary-Layer Meteorol., 73:159-182.

Smith, S.D. 1980: Wind stress and heat flux over the ocean in gale force winds. - J. Phys. Oceanogr., 10:709-726.

Smith, S.D. 1988: Coefficients for sea surface wind stress, heat flux and wind profiles as a function of wind speed and temperature. - J. Geophys. Res., 93, C12, 15467-15472.

Smith, S.D. 1989: Water vapour flux at the sea surface. - Boundary-Layer Meteorol., 47:277-283.

REVISION OF THE SURFACE FLUX PARAMETERIZATION OVER THE SEA IN *HIRLAM*: THEORY AND RESULTS

Niels Woetmann Nielsen

Danish Meteorological Institute
Lyngbyvej 100, DK-2300 Copenhagen OE, Denmark

ABSTRACT

The present parameterization in HIRLAM of surface fluxes over the sea does not include the smooth surface regime. Instead, a lower limit is set for the roughness length (currently $1.5 \cdot 10^{-5}$ m). The roughness length for momentum, z_{0M}, is calculated from Charnock's formula, with a constant of proportionality equal to 0.0032. It is further assumed that the roughness lengths for sensible heat and moisture are identical to z_{0M}. Observations as well as theoretical work indicate that this is not the case.

The minimum constraint on z_{0M} together with the applied stability functions ensure that the fluxes of sensible heat and moisture have non-zero values in free convection. However, the latter values depend on the minimum value chosen for z_{0M}. The present formulation in HIRLAM leads to unrealistically small turbulent fluxes of sensible heat and moisture for small mean wind speeds in the surface layer.

The present work describes a revised parameterization scheme in which the shortcomings listed above are eliminated. 1-dimensional results from the revised scheme are compared with results from two alternative schemes. 3-dimensional HIRLAM results are also compared with corresponding results from the original surface scheme. Both the 1- and 3-dimensional experiments show that the surface fluxes over the sea of latent (and sensible) heat generated by the revised scheme are reduced in strong winds and enhanced in light winds.

1. INTRODUCTION

The present parameterization in HIRLAM of surface fluxes over the sea does not include the smooth surface regime. Instead, a lower limit is set for the roughness length (currently $1.5 \cdot 10^{-5}$ m). The roughness length for momentum, z_{0M}, is calculated from Charnock's formula, with a constant of proportionality equal to 0.0032. It is further assumed that the roughness lengths for sensible heat and moisture are identical to z_{0M}. Observations as well as theoretical work indicate that this is not the case.

The minimum constraint on z_{0M} together with the applied stability functions ensures that the fluxes of sensible heat and moisture have non-zero values in free convection. However, the latter values depend on the minimum value chosen for z_{0M}. The present formulation in HIRLAM leads to unrealistically small turbulent fluxes of sensible heat and moisture for small mean wind speeds in the surface layer.

A revised parameterization of surface fluxes over the sea without the shortcomings listed above has been developed for the HIRLAM model. Details about this model are given in Källén, 1996.

2. ROUGH AND SMOOTH SEA SURFACE

In the revised scheme there is a distinction between a smooth and a rough sea. For near-surface wind speeds ≤ 3 m/s the sea is considered to be smooth, with roughness lengths $z_{0\gamma} = r_\gamma \cdot \nu / u_*$ (γ = m (momentum), h (heat) and q (moisture)) with $r_m = 0.11$, $r_h = 0.2$ and $r_q = 0.3$. For near-surface

wind speeds ≥ 5 m/s the sea is considered to be rough, with $z_{0m} = \beta \cdot u_*^2 / g$ (Charnock's relation) with $\beta = 0.014$ over the open sea and $\beta = 0.032$ in coastal waters (fraction of sea ≤ 1). In the transition zone an interpolation formula depending on wind speed is applied. In the rough regime the roughness lengths for heat and moisture are given by (Garratt, 1992)

$$\ln \frac{z_{0m}}{z_{0h}} = c_h Re_*^{1/4} - 2, \tag{1}$$

$$\ln \frac{z_{0m}}{z_{0q}} = \ln \frac{z_{0m}}{z_{0h}} - c_q Re_*^{1/4}, \tag{2}$$

in which Re_* (the roughness Reynolds number) is defined as

$$Re_* = \frac{z_{0m} u_*}{\nu} \tag{3}$$

Over rough sea $c_h = 2.48$, $c_q = 0.20$ and over smooth sea $c_h = 2.43$, $c_q = 0.70$.

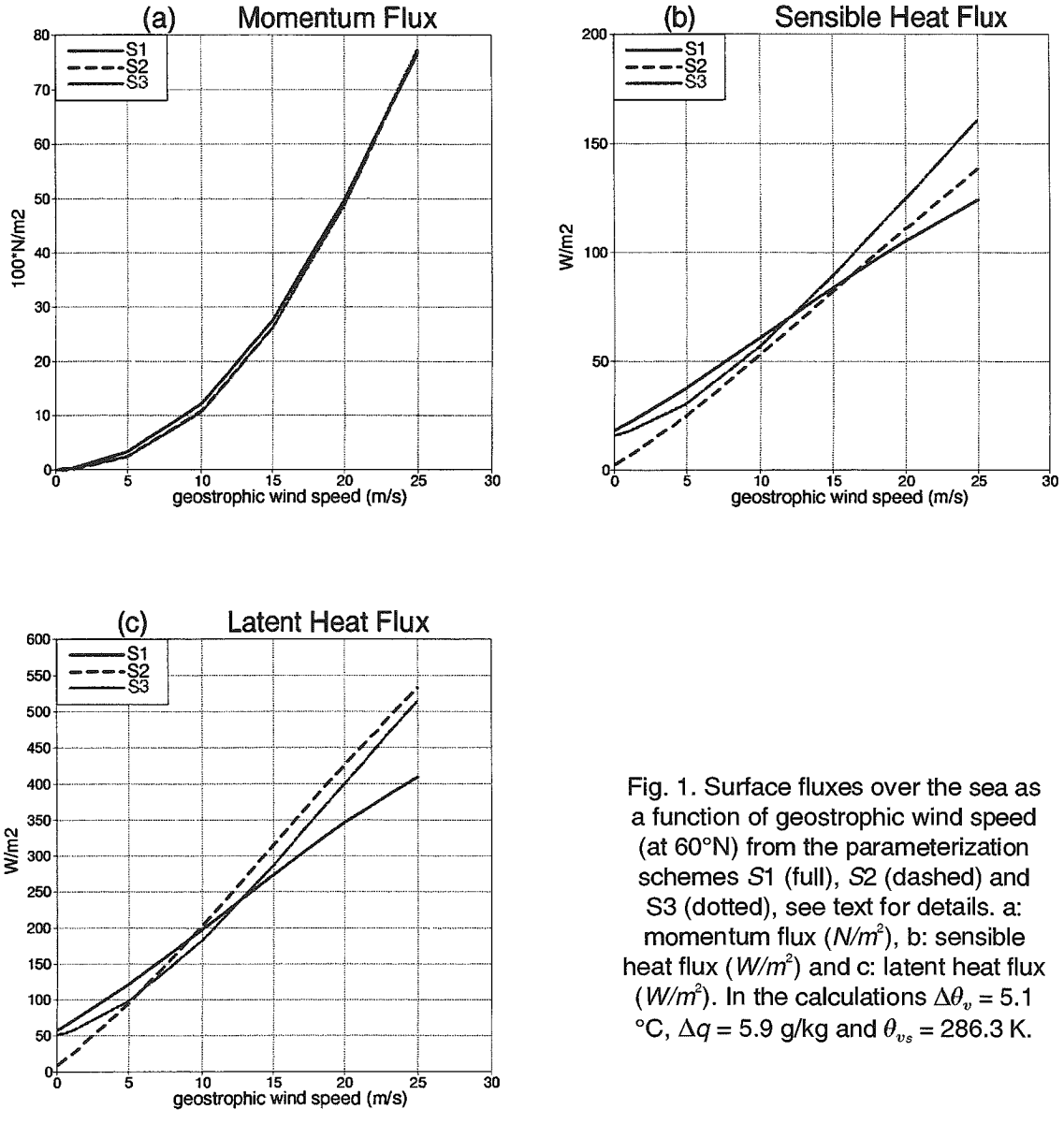

Fig. 1. Surface fluxes over the sea as a function of geostrophic wind speed (at 60°N) from the parameterization schemes *S1* (full), *S2* (dashed) and S3 (dotted), see text for details. a: momentum flux (N/m^2), b: sensible heat flux (W/m^2) and c: latent heat flux (W/m^2). In the calculations $\Delta\theta_v = 5.1$ °C, $\Delta q = 5.9$ g/kg and $\theta_{vs} = 286.3$ K.

3. FREE CONVECTION AND 1D RESULTS

A free convection limit in accordance with laboratory measurements (e.g. Deardorff & al., 1969) is obtained by modifying the stability function in (4) (Louis & al., 1981)

$$f_\gamma = 1 + \frac{a_\gamma \cdot Ri}{1 + b_\gamma \cdot C_{mN} \cdot (Ri \cdot z / z_{0m})^{1/2}} \tag{4}$$

in which a_m=6, a_h=a_q=9 and b_γ=45, Ri is a surface layer bulk Richardson number and C_{mN} the momentum drag coefficient in neutral stratification.

The modification to the stability function in (4) consists of a replacement of C_{mN} with $C_{\gamma N}$ and z_{0m} in the square root term with another length scale d_γ. The definition of $C_{\gamma N}$ is

$$C_{\gamma N} = C_{mN} \left(1 + \ln \frac{z_{0m}}{z_{0\gamma}} / \ln \frac{z}{z_{0m}} \right)^{-1}, \tag{5}$$

and the definition of d_γ is

$$d_\gamma = \left(\delta_H \cdot \mathrm{Pr}^{-2/3} \cdot e_\gamma \right)^2 \cdot \nu / u_{FC}, \tag{6}$$

in which $\delta \approx 0.17$, Pr is the Prandtl number, ν is the molecular kinematic coefficient of viscosity, e_γ is a constant ($e_m = 7.5 \cdot Pr^{4/3}$, $e_h = e_q = 5.$) and $u_{FC} = (g/\theta_v \cdot \Delta\theta_v \cdot \nu)^{1/3}$. Figure 1 shows an example of surface momentum, heat and moisture (latent heat) fluxes, as a function of geostrophic wind speed, produced by the revised scheme (S1) in a 1-dimensional (1D) version of HIRLAM. For comparison the figure also includes results from two alternative parameterizations, i.e., Makin & Perov, 1997 (S2) and Miller & al., 1992 (S3). Further information about the revised scheme in HIRLAM is given in Nielsen, 1998.

4. 3D RESULTS

The revised formulation (*S*1) has been tested in HIRLAM 4.2 for extended periods, including the FASTEX period in February 1997 and a summer period in 1998 (1 July to 13 August). The experiments have been run in parallel with a version of HIRLAM 4.2 applying the unmodified surface flux scheme (*S*0). For the data shown in Figure 2 the applied horizontal and vertical resolution was 0.4° and 22 levels, respectively. The 3D parallel experiments confirm the results obtained in the 1D experiments (Figure 1). In strong winds the surface fluxes of sensible and latent heat are considerably reduced in the revised scheme. A typical example for the surface latent heat flux is shown in Figure 2a. On the day shown, relatively cold air has been advected over the North Sea by near-surface winds in the range from 15 to 25 m/s. At the valid time of Figure 2a the latent heat flux forecasted by the unmodified scheme, *S*0, was typically in the range from 100 to 200 W/m^2 over the North Sea (figure not shown). In *S*1 these fluxes have been reduced by 10 to 40 W/m^2.

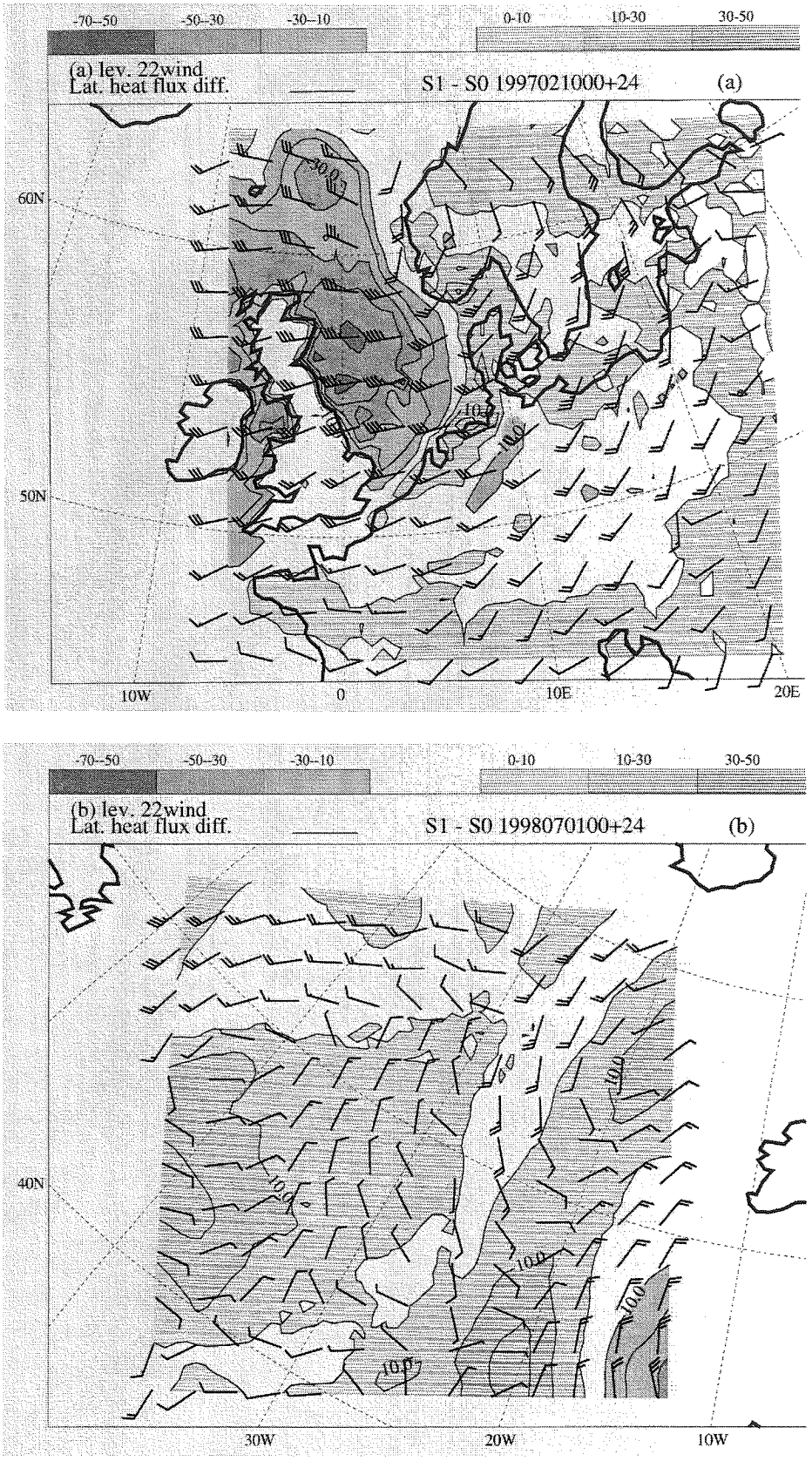

Fig. 2. Difference *S*1-*S*0 in surface latent heat flux for two parallel forecasts *S*1 and *S*0 (see text for details) together with wind velocity (WMO standard) at the lowest model level in *S*1. Negative flux differences (≤-10 W/m^2) are shaded and positive differences are hatched. The contour interval is 10 W/m^2. a: 24 hours forecast from 00 UTC, 10 February 1997, b: 24 hours forecast from 00 UTC, 1 July 1998.

An example of the enhancement of the surface latent heat flux by *S*1 in light winds is shown in Figure 2b. In this case the integration domain was centred at 50°N, 30°W over the central North Atlantic. The fluxes are 10 to 20 W/m^2 higher in *S*1 in regions with weak, mainly anticyclonic, flow. In these regions the fluxes in *S*1 were typically between 30 and 70 W/m^2 (figure not shown).

In the long-term integrations (period 1 July to 13 August) differences of -2 to +2 hPa in the average mean sea level (msl) pressure patterns for *S*1 and *S*0 were found. These differences are of the same order of magnitude as the typical msl pressure bias found on a monthly basis in verification against observations over Europe.

The long-term integrations also showed that the effect of the change in surface flux parameterization was spread through the whole atmosphere. An indication of this process was a clear negative correlation between the thickness fields of the troposphere (1000-850 hPa, 850-500 hPa, 500-300 hPa) and the stratosphere (300-100 hPa) (figures not shown).

5. DISCUSSION

The revised scheme *S*1 can be regarded as a first step in the process of improving the parameterization of turbulent surface fluxes over the sea. An accurate parameterization of these fluxes is of primary importance in climate simulations, but due to their significant impact on the evolution of the atmospheric boundary layer and on cyclogenesis over the sea, this accuracy is also required in short-range weather forecasting.

The scheme could probably be further improved by including in z_{0M} a dependence of wave age c_f/u_* (c_f being the phase speed at the peak of the ocean wave spectrum and u_* the surface friction velocity). However, such a step requires a coupling of the atmospheric model to an ocean wave model. Furthermore, the scheme does not take into account impacts on the surface fluxes by processes or dependencies such as sea spray (at high wind speeds), precipitation and variation of $q_{sat}(T_s)$ with salinity.

Makin, 1998, has demonstrated the significant impact of sea spray on surface fluxes of sensible and latent heat at wind speeds in excess of 25 m/s in a numerical model of the marine surface layer (including interaction with sea waves).

In numerical models of tropical hurricanes it has been found that the moisture exchange coefficient must be comparable in magnitude to the momentum drag coefficient in order to obtain the observed intensities of tropical hurricanes. This is another indication of an enhancement of the moisture flux by sea spray at very high wind speeds in an unstable stratified boundary layer.

References

Deardorff, J.W., Willis, G.E. & Lilley, D.K. 1969: Laboratory investigation of non-steady penetrative convection. - J. Fluid Mech. 35:7-31.

Louis, J.F., Tiedtke, M. & Geleyn, J.F. 1981: A short history of the PBL parameterization at ECMWF. - In: ECMWF Workshop on Boundary-Layer Parameterization, p. 59-79.

Garrat, J.C., 1992: The atmospheric boundary layer. - Cambridge University Press, 316 pp.

Källén, E. (ed.) 1996: HIRLAM Documentation Manual: system 2.5. - Technical report, SMHI, Norrköping, Sweden.

Makin, V.K., 1998: Air-sea exchange of heat in the presence of wind waves and spray. - J. Geophys. Res. 103:1137-1152.

Makin, V.K. & Perov, V., 1997: On the wind speed dependence of momentum, sensible heat and moisture exchange coefficients over sea in the HIRLAM model - a case study. - HIRLAM Newsletter 29:26-31.

Miller, M.J., Beljaars, A.C.M. & Palmer, T.N., 1992: The sensitivity of the ECMWF Model to the parameterization of evaporation from the tropical ocean. - J. Climate 5:418-434.

Nielsen, N.W., 1998: Inclusion of free convection and a smooth sea surface in the parameterization of surface fluxes over sea. - HIRLAM Newsletter 32:44-51.

No. 40

Workshop on modelling of the marine-atmospheric boundary layer

Merentutkimuslaitos
Lyypekinkuja 3 A
PL 33
00931 Helsinki

Havsforskningsinstitutet
PB 33
00931 Helsingfors

Finnish Institute of Marine Research
P.O. Box 33
FIN-00931 Helsinki, Finland

ISSN 1238-5328 ISBN 951-53-2078-X